

Coronary Artery Tracking with Rule-based Gap Closing

DIPLOMARBEIT

zur Erlangung des akademischen Grades

Diplom-Ingenieur

im Rahmen des Studiums

Medizinische Informatik

eingereicht von

Andreas Grünauer

Matrikelnummer 0305179

an der
Fakultät für Informatik der Technischen Universität Wien

Betreuung

Betreuer: Ao.Univ.Prof. Dipl.-Ing. Dr.techn. Eduard Gröller

Mitwirkung: Dipl.-Math. Dr.techn. Katja Bühler und Dr.techn. Sebastian Zambal

Wien, 04.07.2011

(Unterschrift Verfasser)

(Unterschrift Betreuer)

Erklärung zur Verfassung der Arbeit

ANDREAS GRÜNAUER

Rapfstrasse 16

2020 Hollabrunn, ÖSTERREICH

Hiermit erkläre ich, dass ich diese Arbeit selbständig verfasst habe, dass ich die verwendeten Quellen und Hilfsmittel vollständig angegeben habe und dass ich die Stellen der Arbeit – einschließlich Tabellen, Karten und Abbildungen –, die anderen Werken oder dem Internet im Wortlaut oder dem Sinn nach entnommen sind, auf jeden Fall unter Angabe der Quelle als Entlehnung kenntlich gemacht habe.

Wien, am 4. Juli 2011

.....

(Unterschrift Verfasser)

Abstract

Coronary artery diseases are among the leading causes of death in the industrial countries. The high death rate leads to an increased demand of diagnosis and treatment of these diseases. Additional to the conventional coronary angiography, the CT angiography is mainly used in the extended diagnostics of coronary artery diseases. This modality allows a detailed assessment of the coronary vessels and potentially present stenoses. For supporting the radiologist during the evaluation of the coronary arteries by the help of computer-aided diagnostic methods, robust and efficient procedures for the tracking of coronary arteries are needed.

The approach presented in this thesis unifies the strong points of existing methods delivering high accuracy with the strong points of methods achieving high overlap. Therefore the approach presented in this thesis aims at highly accurate results in combination with high overlap of the investigated coronary artery vessel tree. The approach is divided into three phases: 1) calculation of seed points, 2) tracking of vessel segments, and 3) construction of the coronary artery trees.

Phase 1 & 2 are executed in an automatic manner. First potential seed points for the tracking of vessel segments are identified. During the second phase, vessel segments located at these seed points are tracked by use of a cylindrical shape model. By use of rule-based anatomical heuristics, the third and final phase combines vessel segments to form complete coronary artery trees. This phase requires minimal user interaction, as the location of the root of the left and right coronary artery tree needs to be specified.

Beside the detailed description of the algorithm, the integration into a professional radiology workstation is demonstrated. The results obtained by the evaluation on 24 CTA datasets show a high overlap (OV) of 89.5% in combination with very precise accuracy (AI) of 0.24 mm in comparison to an expert-annotated reference segmentation.

Kurzfassung

Die koronare Arterienkrankheit gehört zu den häufigsten Todesursachen in den Industrieländern. Die hohe Sterblichkeitsrate führt zu einer erhöhten Nachfrage nach Diagnose und Behandlung dieser Krankheiten. In der erweiterten Diagnose von Erkrankungen der Koronararterien kommt zusätzlich zu der konventionellen Koronarangiographie die CT-Angiographie vermehrt zum Einsatz. Diese Modalität ermöglicht eine detaillierte Beurteilung der Herzkranzgefäße sowie eventuell vorhandener Stenosen. Um den Radiologen bei der Analyse von Koronararterien mittels computerunterstützter Diagnostik zu unterstützen, sind robuste und effiziente Verfahren zur Erfassung des Koronararterienverlaufs gefragt.

Der vorgestellte Ansatz vereint die Stärken von Methoden, die hohe Genauigkeit erreichen mit Stärken von Methoden, die einen hohen Grad an Gefäßüberlappung erzielen. Der vorliegende Ansatz zielt somit auf hochgenaue Ergebnisse in Kombination mit einem hohen Überlappungsgrad der untersuchten koronaren Gefäßbäume und ist in drei Phasen unterteilt: 1) Berechnung von Initialisierungspunkten, 2) Erfassung von Gefäßsegmenten und 3) Zusammenführung der Gefäßsegmente zu koronaren Gefäßbäumen.

In Phase 1 werden Initialisierungspunkte innerhalb von Blutgefäßen berechnet, die in Phase 2 als Ausgangspunkte für die Erfassung von Gefäßsegmenten mittels zylindrischer Formmodelle dienen, wobei beide Phasen vollautomatisch ablaufen. Durch den Einsatz einer regelbasierten, anatomischen Heuristik werden in Phase 3 die erfassten Gefäßabschnitte zu vollständigen koronaren Gefäßbäumen zusammengesetzt. Diese Phase erfordert eine minimale Benutzerinteraktion, um jeweils die Wurzel des linken und rechten koronaren Gefäßbaums zu lokalisieren.

Neben der detaillierten Beschreibung des Algorithmus wird auch dessen Integration in eine professionelle radiologische Arbeitsumgebung demonstriert. Die durch die Auswertung von 24 CTA Testdatensätzen erhaltenen Resultate bestätigen einen hohen Überlappungsgrad (OV) von durchschnittlich 89.5% bei einer sehr hohen Genauigkeit (AI) von durchschnittlich 0.24 mm im Vergleich zu einer von Experten annotierten Referenzsegmentierung.

Contents

1	Introduction	1
1.1	Medical Background	1
1.1.1	Anatomy and physiology of the coronary arteries . . .	1
1.1.2	Pathologies (coronary artery disease)	2
1.1.3	Imaging procedures	3
1.1.4	Diagnosis	3
1.1.5	Questions to the image	4
1.2	Visualization techniques	4
1.3	Problem statement	8
1.4	Requirements	8
1.5	Goal of the thesis	8
2	Related Work	9
2.1	Vessel structure extraction	10
2.1.1	Pattern recognition techniques	10
2.1.2	Model-based approaches	11
2.2	Merging of discontinuities in vessel structures	12
2.3	Conclusion	13
3	The starting points	15
3.1	Tracking method of Zambal et al.	15
3.1.1	Detection of coronary artery seeds	15
3.1.2	Vessel tracking	17
3.2	Tree connection method of Bauer et al.	24
3.3	Discussion (critic) of existing approaches	25
4	The end point: The best of two worlds	27
4.1	Phase 1: Calculation of seed points	27
4.1.1	Calculation of the heart mask	28
4.1.2	Calculation of seed points	29
4.2	Phase 2: Vessel segment tracking	32
4.3	Phase 3: Topological tree growing	36

4.3.1	Connection rules	36
4.3.2	I-Connection rule	38
4.3.3	T-Connection rule	39
4.3.4	Y-Connection rule	42
4.3.5	Tangent estimation	45
4.3.6	Tree growing main algorithm	46
4.3.7	Sub-tree search algorithm	48
5	Implementation	51
5.1	Parameters and connection rules	51
5.1.1	I-Rule	53
5.1.2	I-Rule-StrongBend	53
5.1.3	T-Rule	53
5.1.4	Y-Rule-SmallDist	53
5.1.5	Y-Rule-MediumDist	54
5.1.6	Y-Rule-LargeDist	54
5.2	Hardware and performance	54
6	Results	55
6.1	Evaluation Framework	55
6.1.1	Training and test datasets	55
6.1.2	Evaluation measures	56
6.1.3	Scoring & ranking of the algorithms	58
6.1.4	Algorithm categories	58
6.2	Results	60
6.2.1	Overlap results	60
6.2.2	Accuracy results	62
6.3	Comparison to base approach	64
6.3.1	Improvements	64
6.3.2	Tracking issues	68
6.3.3	Rule issues	70
6.4	Results on other medical data	71
7	Integration in medical software	77
7.1	Graphical user interface	77
7.1.1	3D vessel surface mesh rendering	78
7.1.2	MPR views	79
7.1.3	3D volume rendering	79
7.2	Workflow	81
7.2.1	(Semi-)automatic tracking	81
7.2.2	Single-click vessel tracking	81

8 Conclusion and Future Work	83
Bibliography	85

List of Figures

1.1	Anatomy of the heart	2
1.2	CTA dataset in DVR	5
1.3	CTA dataset in MIP	6
1.4	CPR visualization	7
3.1	Coronary arteries origin	16
3.2	Sample patterns of cylindrical shape model	18
3.3	Straight cylindrical shape vs. bent shape	19
3.4	Local histograms	20
3.5	Scheme for generating of shape configurations	21
3.6	Coronary artery centerline interpolation	24
4.1	Results of the three phases of algorithm	27
4.2	Calculation of the heart mask	28
4.3	Calculation of seed point	32
4.4	I-Connection rule	38
4.5	T-Connection rule	41
4.6	T-Connection rule branch angles	42
4.7	Y-Connection rule	44
4.8	Node paths with different degrees of straightness	45
4.9	Mean angle of nodepath	46
6.1	Overlap measures of all 24 test datasets	61
6.2	Accuracy inside vessel (AI) measures of all 24 test datasets.	63
6.3	Comparison of evaluated measures	65
6.4	Dataset 26: Results of the three phases of the algorithm	67
6.5	Dataset 26: Comparison of extracted centerlines	68
6.6	Dataset 11: Results of the algorithm, incl. comparison	69
6.7	Dataset 20 & 27: Premature termination of vessel tracking	72
6.8	Results on other CTA dataset	73
7.1	GUI of the vessel tracking tracking plug-in	78
7.2	Different modes of 3D volume rendering	80

List of Tables

5.1	Summary of parameter values in implementation	52
5.2	Summary of connection rules	52
6.1	Summary of the evaluation measures of the 24 test datasets. .	60
6.2	Average overlap measures of the 24 test datasets.	62
6.3	Accuracy inside vessel (AI) measures of the 24 test datasets. .	63
6.4	Results per vessel of test datasets 8-19	74
6.5	Results per vessel of test datasets 20-31	75

Chapter 1

Introduction

Coronary artery diseases are among the most prominent causes of premature death in the industrial countries [4, 21]. The high death rate leads to an increased demand of diagnosis and treatment of these diseases. Additional to the conventional coronary angiography, the CT angiography is mainly used in the extended diagnostics of coronary artery diseases. This modality allows a detailed assessment of the coronary vessels and potentially present stenoses. For supporting the radiologist during the evaluation of the coronary arteries by the help of computer-aided diagnostic methods, robust and efficient procedures for the tracking of coronary arteries are needed.

1.1 Medical Background

For a better understanding of the importance and diagnostic aspects of the coronary artery diseases, the following chapter provides an overview of the anatomy, physiology and pathology of the coronary arteries. Additionally an overview on diagnosis and visualization techniques is given.

1.1.1 Anatomy and physiology of the coronary arteries

The two main coronary arteries (CA) are the left coronary artery (LCA) and the right coronary artery (RCA). They branch off from the aorta just before it leads into the left ventricle. A schematic illustration of the heart and the coronary arteries is shown in figure 1.1.

The coronary arteries supply the heart muscle with fresh, oxy-

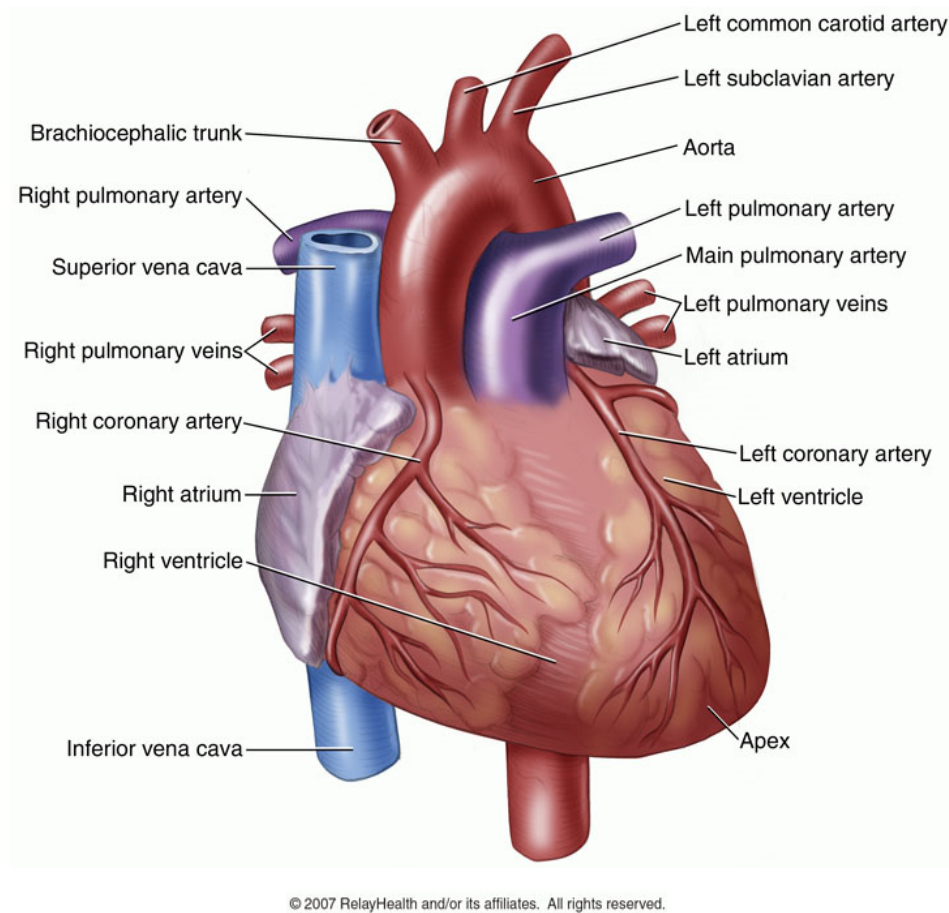


Figure 1.1: Schematic illustration of the heart and the coronary arteries.
 Copyright ~©2010 RelayHealth and/or its affiliates. All rights reserved.

generated blood. The RCA supplies the right part of the heart. The LCA supplies the left part of the heart and usually splits up into the left anterior descending (LAD) and the left circumflex (LCX) arteries. The normal diameter of coronary arteries at the ostium is about 5 mm. The clinical relevant part of a coronary artery vessel is the part from the ostium up to the location where the diameter drops below 1.5 mm.

1.1.2 Pathologies (coronary artery disease)

As mentioned previously, the coronary artery disease is the leading cause of morbidity and mortality in the industrial world. The underlying process of the coronary artery disease is atherosclerosis, which is a

systemic disease of the arterial vessel wall [4]. The vessel wall thickens due to the successive accumulation of lipids and other materials like i.e. macrophages and calcium. These lesions (plaques) develop silently over years and may lead to clinical problems if the accumulation exceeds a certain degree. The narrowing of the vessel lumen (stenosis) leads to a decrease of blood flow, which causes an under-supply of the affected myocardium with oxygenated blood. If the under-supply of the muscle is permanent, more and more muscle cells die (necrosis). Consequences are myocardial infarctions, cardiac insufficiency and arrhythmias (irregular heart beats).

1.1.3 Imaging procedures

Gold standard in the field of the diagnostics of the coronary artery disease is the conventional coronary angiography (CCA). Iodinated contrast agent is applied by insertion of a catheter to the vascular system. Vessels filled with contrast agent are made visible using a fluoroscope. Advantages of this method are long-term well-documented evidence of coronary diagnostics and a very high spatial and temporal resolution compared to other imaging options [17].

Modern multidetector row computed tomography (MDCT) with up to 64 slices revealed new applications for computed tomography in the field of cardiologic imaging. One of these applications is Computed Tomography Angiography (CTA) which is considered as a non-invasive alternative to CCA. An advantage of the CTA is that - other than the conventional coronary angiography - the results show not only the vessel lumen, but also the vessel wall and spots of calcification.

1.1.4 Diagnosis

Given the suspicion of coronary artery disease, the basic diagnostics like anamnesis, clinical study, laboratory tests, resting and exercise electrocardiography and echocardiography help to assess the presence of a treatment-requiring coronary artery disease. If the basis diagnostics delivers normal results, extracardiac causes are further investigated.

In the case that the patient belongs to a certain at-risk group and the basis diagnostics led to suspect or ambiguous results, an exercise echocardiography is carried out. If this investigation shows pathological

results, a coronary angiography is necessary.

Pathologic results of exercise echocardiogram or with different forms of Angina pectoris (typical, instable or at low exercise) indicate a high probability of a present coronary artery disease. In this case the coronary angiography is needed for the determination of the therapy strategies.

1.1.5 Questions to the image

Due to the mentioned indications of coronary CTA, the radiologists have following questions on the image retrieved by coronary CTA [10].

- Detection of significant coronary artery stenoses
- Detection and characterization of both calcified and non-calcified plaque

1.2 Visualization techniques

Appropriate software can support the radiologist to answer the stated questions on coronary CTA data sets. The following visualization techniques exist [10]:

- Volume Rendering (for the detection of coronary artery anomalies and cardiac surgery planning)
- Maximum intensity projection (MIP)
- Multiplanar reformation (MPR)
- Curved planar reformation (CPR)

Figure 1.2 shows a CTA dataset in volume rendering. Figure 1.3 shows the same dataset using MIP.

One way to visualize small tubular structures like the coronary arteries is the technique of Curved Planar Reformation (CPR) [11]. The principle of this technique is shown in figure 1.4(a). Given the image data and the pathway of the vessel centerline (red colored), CPR generates a longitudinal profile of the vessel. The resulting image shows information about the vessel lumen, wall thickness and surrounding tissue along a curved plane. Figure 1.4(b) shows a CPR of the right

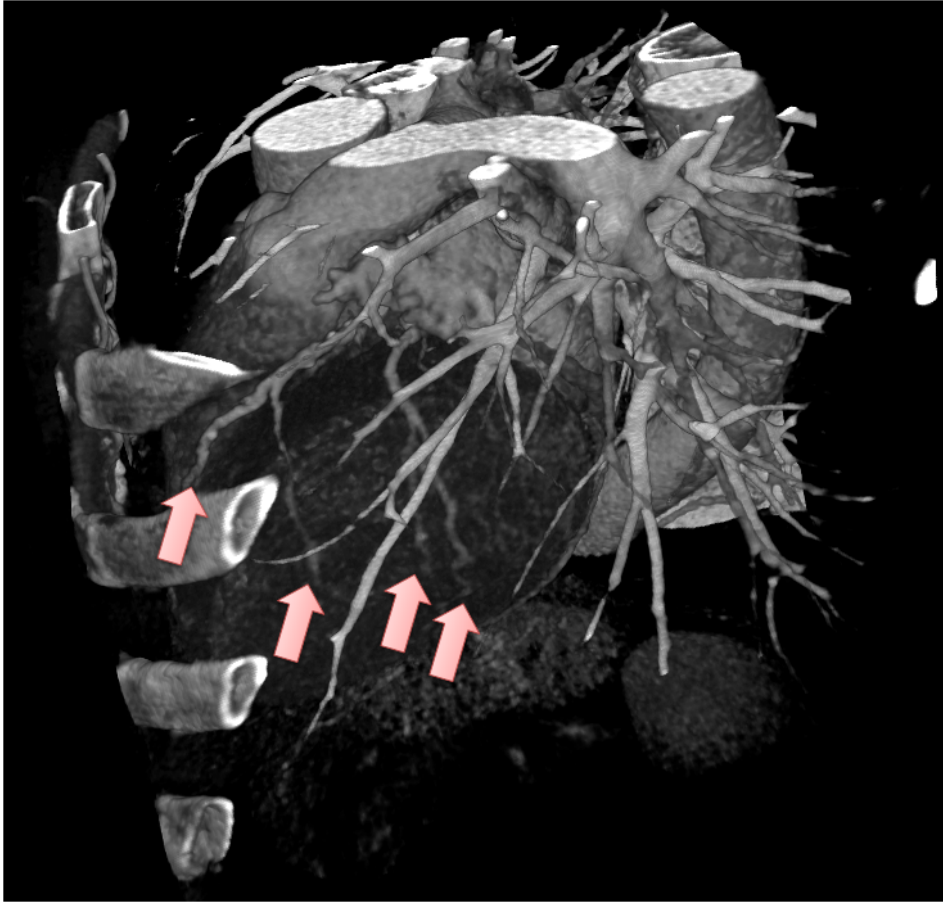
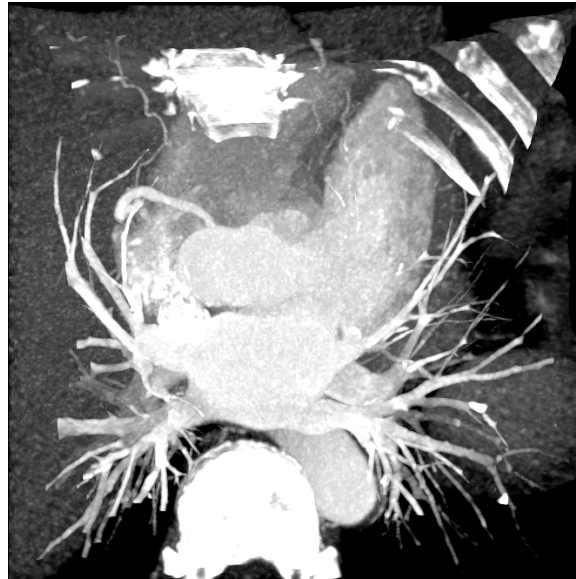


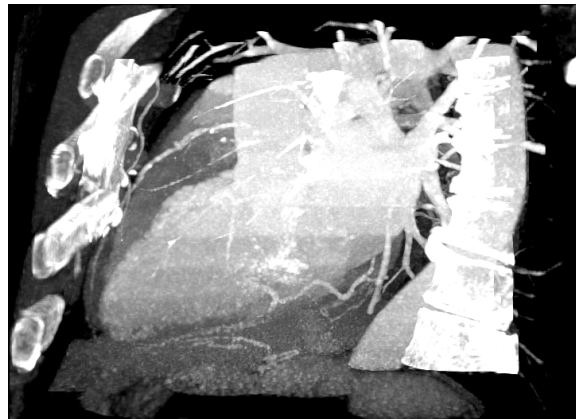
Figure 1.2: CTA dataset in DVR. The red arrows mark vessels of the left coronary artery tree.

coronary artery that demonstrates high-grade stenoses of the proximal segment (arrow) and nonsignificant stenoses of the mid and distal segments (arrowheads).

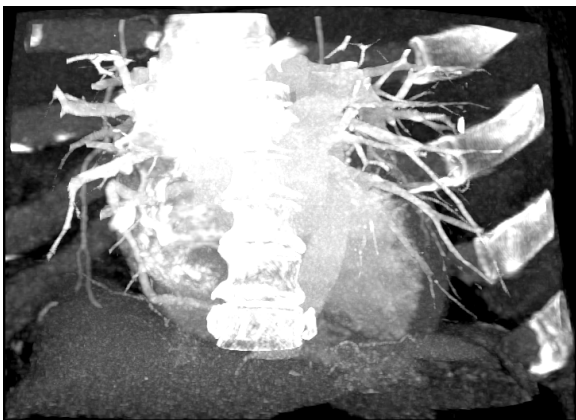
A prerequisite of the CPR is the pathway of the central lumen line (centerline) of the observed vessel. These centerlines can be created manually or by the use of centerline extraction algorithms (vessel tracking) and serve as the basis for visualization techniques for the coronary artery disease like the approach of Termeer et al. [26]. The computer-aided extraction of vessel centerlines potentially saves the amount of physician time required for each study. The gained increase in efficiency can help to deal with the rising demand of coronary artery disease diagnostic.



(a)

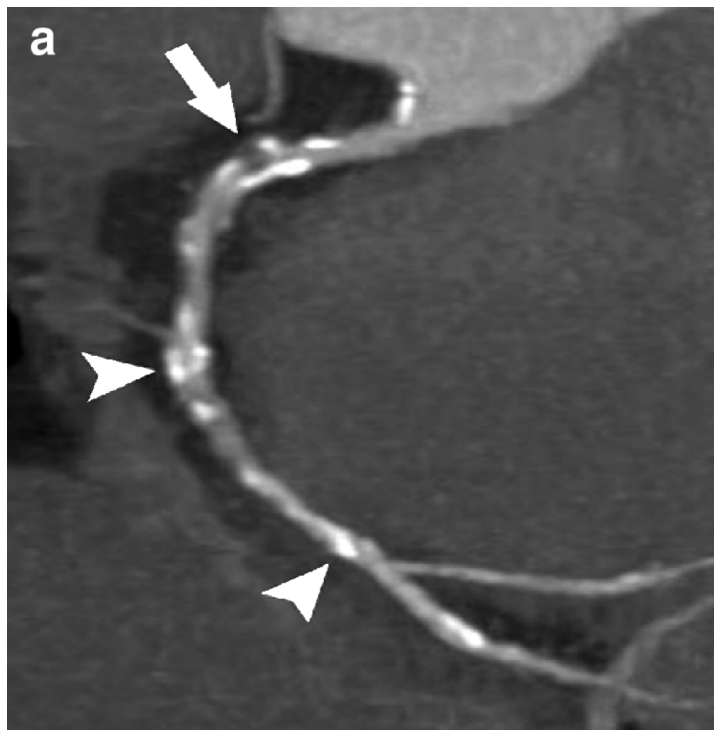
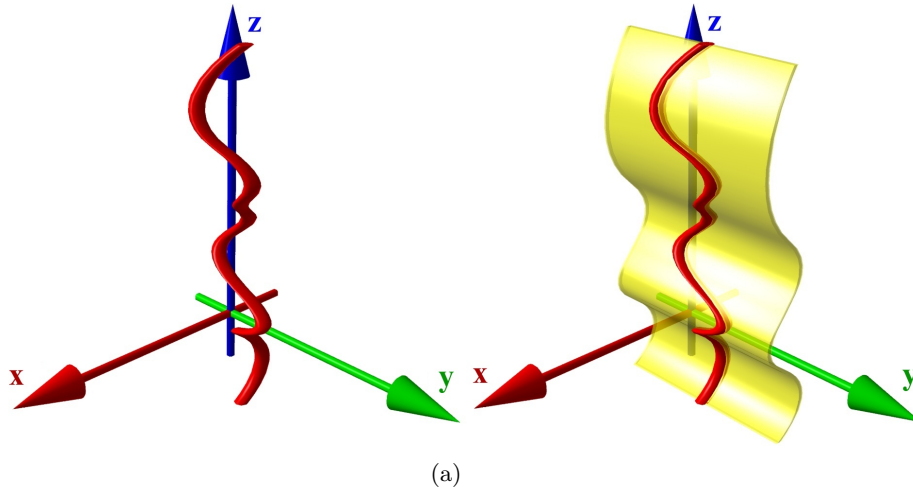


(b)



(c)

Figure 1.3: CTA dataset in MIP: (a) axial view, (b) sagittal view, (c) coronal view.



(b)

Figure 1.4: (a) Principle of the CPR visualization technique. Figure from [11]., (b) CPR of the RCA demonstrates high-grade stenoses of the proximal segment (arrow) and nonsignificant stenoses of the mid and distal segments (arrowheads). Figure from [23].

1.3 Problem statement

The problem is to extract the centerlines and according radii of the vessel lumen of coronary arteries on CTA datasets. This is a challenging task because of

- Modality inherent noise [9]
- Motion artifacts of the beating heart.
- High variations of vascular anatomy
- Low spatial resolution in proportion to coronary artery diameter
- Areas of calcification with high contrast in respect to the vessel lumen can lead to wrong centerlines

1.4 Requirements

The result of a centerline extraction algorithm should capture the coronary arteries well (high overlap). A resulting centerline should also match as close as possible with the "real" centerline of the investigated vessel (high accuracy). For the use as an efficiency-raising tool, a centerline extraction algorithm should also require as minimal user interaction as possible.

1.5 Goal of the thesis

The goal of the thesis is to combine the strengths of existing methods delivering high accuracy with methods achieving high overlap. Therefore the approach presented in this thesis aims to achieve highly accurate results by on the same time obtaining a high overlap of the investigated coronary artery vessel tree.

Chapter 2

Related Work

Tracking of coronary arteries is a special case of vessel extraction. A wide range of different vessel segmentation and/or centerline extraction approaches have been published. The papers of Kirbas et al. [13] and Lesage et al. [15] give a broad review on the classification of existing works, each proposing different classification schemes.

The survey of Kirbas et al. [13] follows a rather linear discrimination of different vessel extraction techniques, which are divided into six main categories:

- Pattern recognition techniques
- Model-based approaches
- Tracking-based approaches
- Artificial intelligence-based approaches
- Neural network-based approaches
- Miscellaneous tube-like object detection approaches

Lesage et al. [15] discuss existing extraction approaches according to three aspects:

- Appearance & geometric models
- Image features
- Extraction schemes

The following chapter will give an overview of related work in the field of vessel extraction and then presents approaches which explicitly handle the treatment of disconnected vessel segments.

2.1 Vessel structure extraction

2.1.1 Pattern recognition techniques

According to Kirbas et al. [13], the category of pattern recognition techniques in the field of vessel extraction deals with the automatic detection of vessel structures and vessel features.

Multi-scale approach

The analysis of second-order derivatives or the Hessian matrix of the image is a common technique in the field of vessel filtering and tracking. Frangi et al. proposed a multiscale vessel enhancement filtering based on the analysis of the Hessian's eigenvectors. Multiscale-based approaches have been presented by Tek et al. [25], Yang et al. [27], Krissian et al. [14] and Metz et al [18].

Region growing

Beginning from an initial seed point, approaches based on region growing successively recruit voxels to a region according to certain predefined criteria like value similarity and spatial proximity. Examples for region growing approaches are the methods of Eiho et al. [7] and Bock et al. [3]. Also the already mentioned approach of Metz et al. [18] uses region growing techniques.

Ridge-based

Ridge-based approaches interpret grayscale images as elevation maps, where intensity ridges represent approximations for the skeleton of tubular structures [1].

The method of Bauer et al. [2] uses a height ridge traversal procedure on the result of a Gradient Vector Field (GVF) transformation. Section 3.2 contains a detailed description of this method.

The ridge-based algorithm of Szymczak [24] extracts persistent maxima of the intensity out of 2D axis-aligned slices of the volume data.

These maxima are supposed to concentrate along 1D intensity ridges. The algorithm creates a forest of vessel sub-trees by connecting nearby persistent maxima. The resulting forest contains numerous spurious features and fails to connect segments in low contrast areas. Therefore simple geometric heuristics are used to trim short branches, fill gaps in areas of low contrast and remove spurious branches.

Mathematical morphology schemes

Mathematical morphology denotes the processing of geometrical structures founded on the set theory. Morphological operations like Dilation and Erosion apply structuring elements to the image data. Dilation expands the objects of the image, whereas erosion reduces them. Approaches based on Mathematical morphology are presented by Bouraoui et al. [5], Luengo-Oroz et al. [16] and Castro et al. [6].

2.1.2 Model-based approaches

Model-based approaches apply explicit vessel models to extract the vascular structures. These vessel models embed prior knowledge about the target structure.

Zambal et al. [28] use cylindrical shape and appearance models. First a heart-model is fitted to identify the region of the coronary artery ostia to reduce computational complexity and to avoid tracking of vessels in non-cardiac areas. Local symmetry feature extraction returns potential seed points of the roots of the coronary artery trees. A curved cylindrical shape model is successively matched along vessel structures especially designed for matching strongly bended structures. The basic assumption of the model alignment is that assuming a perfect match of the model, the histogram of the gray values inside the vessel should 'concentrate' in the high area, whereas the mean of the gray values of the exterior samples reside in the lower part of the spectrum. Section 3.1 provides a detailed description of this approach.

The interactive method of Friman et al. [8] uses a model based multiple hypothesis tracking methodology in combination with a standard minimal path search to fill gaps of vessels. This approach achieved the

best results in the interactive category of the MICCAI 2008 workshop, but it is also expensive in terms of the computation time. During tracking, the algorithm iteratively places model segments in front of each other to form a chain of segments representing the vessel trees. This tracking algorithm is based on a 3D vessel template. The vessel template represents an idealized model of a vessel segment and is parametrized by position, radius and orientation. Iteratively, a set of possible vessel continuations is generated based on the current vessel segment. The possible vessel segments are compared based on a score function that measures the fitting quality of a segment on the basis of the underlying image data. The authors propose a multiple hypothesis tracking framework to evaluate several hypothetical vessel trajectories. For each investigated vessel segment a search tree (depth=4) is built by the recursive evaluation of possible vessel continuations. Additionally a minimal path algorithm is used to bridge gaps in areas of low contrast.

2.2 Merging of discontinuities in vessel structures

Although the connection of gaps is a well-known problem in 2D edge detection, far fewer results are published in the corresponding 3D problem. The general idea is to infer the linkage of unconnected parts of the vessel tree from their distance and orientation to each other.

The method of Risser et al. [19, 20] is based on the formalism of tensor voting. It uses vectorial information of the vessel graph to reason about the connection of gaps.

The approach of Kaufhold et al. [12] utilizes both, the geometric properties of the investigated vessel graph and the underlying gray scale information. Assuming that each connection originates from an end point of the vessel graph, a mask within a bounding box around every end point is generated by relaxation of a gray value threshold, until at least one other point of the vessel graph is reached. The mask is reduced by using a paired path length distance transformation. This way the minimal amount of voxels is kept while still linking the investigated end point with the other point. It additionally avoids backtracking to

the centerline of the investigated end point.

The methods of Bauer et al. [2] and Szymczak et al. [24] make use of continuous cost functions between connection candidates. If a connection pair yields a cost value below a given threshold, a connection is created.

The approach of Szymczak [24] considers only the geometrical properties of the investigated leaf vertices of the vessel forest. Two basic assumptions are made: (1) The gaps between leaf vertices tend to be small; (2) The outward pointing tangent vectors of the observed leaf vertex should point in a direction close to the other potential connection vertex and vice versa. The cost function therefore reflects these properties with a distance term and a term expressing the angle between the tangent vectors. The tangent vector of a leaf vertex is estimated by considering the positions of start and end point of a path with prescribed length starting from the leaf vertex. The algorithm further rejects edges that would cause loops in the graph.

The approach of Bauer et al. [2] combines geometrical information (distance and angle between tangent vectors of connection candidates) with the gray value similarity at the positions of the connection candidates. This method is described in section 3.2.

2.3 Conclusion

As already mentioned in section 1.5, this thesis aims at the generation of a new tracking algorithm for coronary centerlines that delivers results of high accuracy and overlap.

The Rotterdam Coronary Artery Algorithm Evaluation Framework, presented during the MICCAI 2008 conference, enables the quantitative comparison of different centerline extraction methods of coronary arteries. This framework was also the basis of assessment for the workshop "3D Segmentation in the Clinic: A Grand Challenge II", that was held during the MICCAI 2008 conference.

The approach of Zambal et. al [28] won the first prize in the fully and semi-automatic category of the mentioned MICCAI 2008 work-

shop, achieving the highest accuracy in both categories. Nevertheless this approach is vulnerable to the early termination of vessels in areas of low local contrast. This reduces the overlap of the investigated vessel trees.

The method of Bauer et al. [2] convinced with the highest degree of overlap in the automatic methods category. The weak point is that the method's results show a significantly lower accuracy level than the method of Zambal et al.

The method presented in this thesis combines the strengths of both methods. The accurate tracking method for vessel segments proposed by Zambal et al. is combined with a “bottom-up” approach for the reconstruction of the coronary artery trees similar to the approach of Bauer et al. By connecting the highly accurate vessel segments across regions of low local contrast a highly accurate method with higher overlap should be achieved.

Chapter 3

The starting points: The methods of Zambal and Bauer

3.1 Tracking method of Zambal et al.

This section presents the basic ideas of the coronary artery tracking method of Zambal et al. [28]. The algorithm can be divided into two major parts: The first part deals with the identification of the two coronary artery origins (ostia), whereas the second part uses these origins as the starting points for the extraction of the vessel tree by the iterative fitting of cylindrical shape patterns. In the following, all introduced parameters are denoted with a capital P with the name of the parameter in the subscript.

3.1.1 Detection of coronary artery seeds

3D model of the heart

The first step for the detection of coronary artery seeds is a rough localization of the origin of the left and right coronary artery tree. The approach uses a 3D model of the heart, based on 2245 manually placed landmark points of a CTA dataset. Additionally the model contains two landmark points \mathbf{L} and \mathbf{R} representing the origins of the coronary artery trees. After the model has been fitted to the dataset, the positions of these points give a first estimator for the location of the ostia.

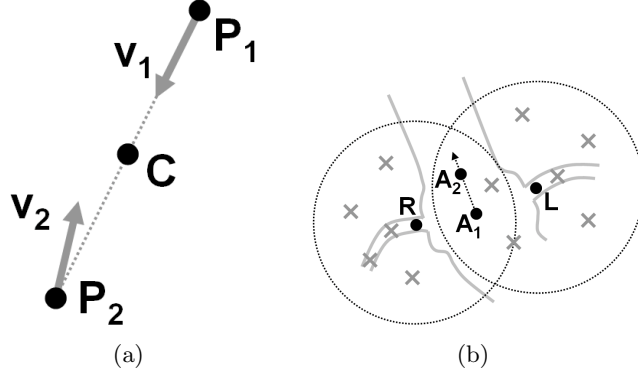


Figure 3.1: (a) Calculation of the symmetry feature along a scan line. (b) Four landmark points (\mathbf{A}_1 and \mathbf{A}_2 inside aorta and \mathbf{L} and \mathbf{R} inside LCA and RCA respectively) define the search regions for the coronary artery origins. Maxima of local symmetry feature (shown as crosses) represent potential origins of the coronary arteries. Figures from [28].

Local symmetry

Due to anatomical variations, points \mathbf{L} and \mathbf{R} will probably not be located on the real coronary artery ostia. Therefore potential coronary artery seeds are searched within a region of radius r_{init} around the points \mathbf{L} and \mathbf{R} , where r_{init} is defined as 2.5 times the distance between the landmark points \mathbf{A}_0 and \mathbf{A}_1 defined in the 3D model of the heart. A local symmetry feature value is calculated for each voxel of the CTA dataset inside this two regions. This symmetry feature computation is based on the assumption that the cross-section of a vessel can be approximated as a circle and therefore contains a lot of symmetry in terms that 3D image gradients along the surface of the vessel profile ideally point towards the center point of the corresponding vessel profile.

Figure 3.1(a) shows the basic idea. First an empty symmetry feature volume is initialized and 3D image gradients are precomputed. For every voxel within the region of interest, the algorithm traverses a scan line along the direction of the related gradient vector \mathbf{v}_1 for a length of 10 mm, which is the expected maximal diameter of coronary arteries. Let \mathbf{P}_1 be the position of the investigated voxel. At every position \mathbf{P}_2 along the scan line a second gradient vector \mathbf{v}_2 is considered. The squared length of the difference between vectors \mathbf{v}_1 and \mathbf{v}_2 is added to the voxel of the feature volume at position \mathbf{C} , which is located in the

middle between \mathbf{P}_1 and \mathbf{P}_2 . Finally, after executing the procedure for every voxel, a fixed number of local maxima of the feature volume are used as potential seed points for the vessel tracking algorithm.

Seed evaluation

The next step evaluates all potential coronary artery seeds and chooses the best two seeds as starting points for the vessel tracking procedure presented in the next section. Each seed is tracked for three iterations and the average vesselness, defined by vesselness function v as described below in section 3.1.2, is calculated. The seed point that exhibits the maximum vesselness is the initial position for the tracking procedure. Figure 3.1(b) illustrates this approach. For selection of the second coronary artery seed, vector \mathbf{a} from \mathbf{A}_1 (a landmark point inside the aorta) to the previous selected seed point is calculated. The next best potential seed point with vector \mathbf{b} from \mathbf{A}_1 to the currently investigated seed point and with an angle greater than 50° between \mathbf{a} and \mathbf{b} is chosen as the second coronary artery seed.

3.1.2 Vessel tracking

The approach of Zambal et al. [28] is build on the successive matching of cylindrical sample patterns of simple symmetric shape, in the following referred to as *shape model*.

Generation of texture samples

Applied on the investigated CTA dataset, the generation of texture samples for a given shape model is determined by position \mathbf{p} , orientation represented by the normalized vector \mathbf{d} and radius r , and is in the following referred to as shape configuration $s(\mathbf{p}, \mathbf{d}, r)$. The texture samples of the shape model within the CTA dataset are generated by translation and scaling of two concentric circles along the orientation vector \mathbf{d} . The bended shape of the shape model is shown in figure 3.2(a) (in cross section) and figure 3.2(b) (in 3D). The pure translation of the inner and outer circle with constant radii would lead to a perfect cylindrical shape that would not fit coronary arteries well enough, as they often show strong curvatures. Figure 3.3 illustrates the difference between the straight cylindrical shape models (top) and curved

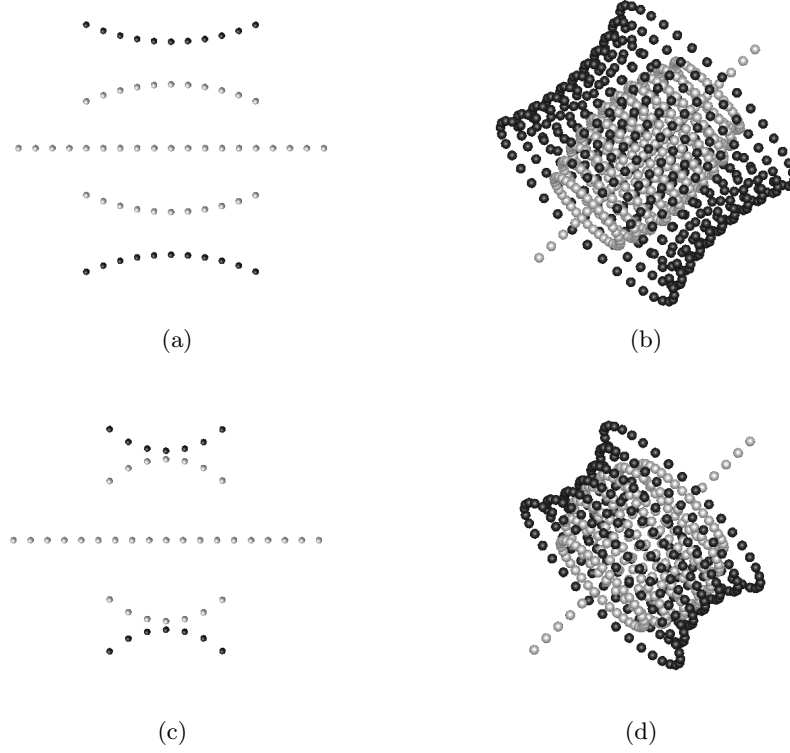


Figure 3.2: Sample pattern one in cross section (a) and 3D (b). Refinement sample pattern two in cross section (c) and 3D (d). Figures from [28].

cylindrical shape models (bottom).

For a given shape configuration $s(\mathbf{p}, \mathbf{d}, r)$, textures are sampled from volume data by positioning and scaling of two concentric (inner and outer) circles at equal distances along the model axis defined by orientation vector \mathbf{d} . The maximal distance between center points of circles and the position \mathbf{p} is equal to radius r . Each circle carries a fixed number of samples, whereby samples on the outer circle represent the background texture and samples on the inner circle represent inner texture of the shape model. For retrieving the previously mentioned bended shape of the shape models, the radii of the circles are scaled by the scaling functions $s_{1,in}$ and $s_{1,ext}$ for generating the inner and outer texture samples for the sample pattern one and the scaling functions $s_{2,in}$ and $s_{2,ext}$ for generating the inner and outer texture samples for the sample pattern two. Hereby, x is defined as the distance between the center point of the circles and point \mathbf{p} .

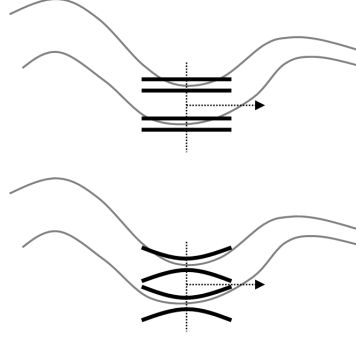


Figure 3.3: Cross section showing the different shapes on a bended structure: straight cylindrical shape model (top), curved cylindrical shape model (bottom). Figure from [28].

The sample textures are generated by using two sample patterns with different level of detail. The first texture pattern is based on quadratic scaling functions

$$s_{1,in}(x) = 0.75 - x^2 * 0.2 \quad (3.1)$$

and

$$s_{1,ext}(x) = 1.25 + x^2 * 0.2 \quad (3.2)$$

and exhibits larger margins between inner and outer texture samples, but less bending. This pattern is used for the rough estimation of the shape configuration, that represents the observed vessel in the dataset. The second texture pattern uses circle-shaped scaling functions

$$s_{2,in}(x) = -0.05 + \sin(\arccos(x)) \quad (3.3)$$

and

$$s_{2,ext}(x) = 2.05 - \sin(\arccos(x)) \quad (3.4)$$

and shows a much smaller margin and a stronger bending, and serves for the further refinement of the roughly estimated shape configuration. For both patterns, additional texture samples (belonging to the class of inner texture samples) are generated along the central axis of the shape model. Figures 3.2(a), 3.2(b), 3.2(c) and 3.2(a) show the position of inner and outer texture samples in gray and black, respectively.

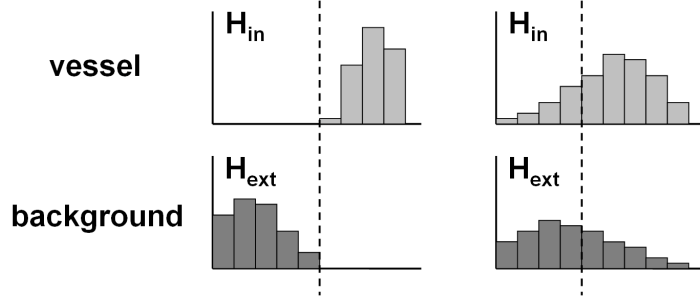


Figure 3.4: Gray value histograms generated from sampled texture of a given shape model. Figure from [28].

Evaluation of texture samples (vesselness)

Given the generated texture samples of a given shape configuration, we now need a way to measure the fitting quality of the shape configuration applied on the observed CTA dataset. This fitting quality is reflected by the vesselness function $v(\mathbf{p}, \mathbf{d}, r)$.

The idea is based on the assumption that both gray value histograms H_{in} and H_{ext} for the inner and outer texture samples are perfectly separable by a certain gray value threshold t , if the given shape configuration matches perfectly the underlying vessel segment. The left part of figure 3.4 shows the case of an ideal match where the inner and outer histograms are perfectly separable by a certain threshold t , indicated as the dashed vertical line, whereas the right part of figure 3.4 visualizes a sub-optimal case where the separation of the histograms is not clear. For the discrimination between these cases of different fitting quality, we use two fractions f_{in} and f_{ext} for each class of the sample textures. Fraction f_{in} is defined as the number of values of histogram H_{in} greater than threshold t divided by the total number of values in H_{in} . Analog, fraction f_{ext} is the number of values of the outer histogram H_{ext} smaller than threshold t divided by the total number of values in H_{ext} . This means that a high fraction value close to 1 indicates a high purity of expected texture values in the class.

Given a shape configuration $s(\mathbf{p}, \mathbf{d}, r)$ and a chosen gray value threshold t , we can calculate the average value of both fractions f_{in} and f_{ext} . The maximization of this average value of both fractions for all possible values of gray value threshold t yields to the value of the vesselness function $v(\mathbf{p}, \mathbf{d}, r)$ for the given configuration.

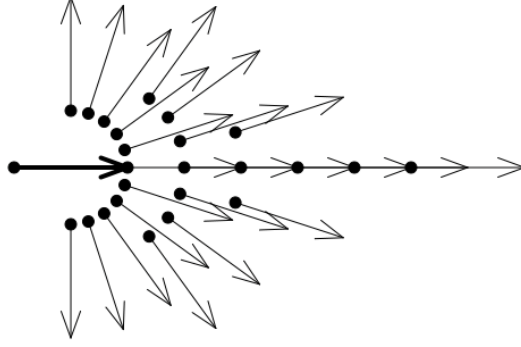


Figure 3.5: Scheme for generating position and directions of shape configurations. Note that close to the direction of the basis shape configuration, the number of generated shape configurations is higher than in the outer regions. Figure from [28].

Tracking of vessels

The presented tracking algorithm works by the iterative extension of the vessel tree with new vessel segments in a depth-first manner. In each iteration, the algorithm generates a set of shape candidates based on the best matching shape configuration of the previous iteration.

The iteration of the tracking algorithm starts with the generation of shape configurations by varying the parameters of the given basis shape configuration s_i . We therefore generate a set of direction vectors $\mathbf{d}_{i,j}$ with angles α relative to \mathbf{d}_i with a step size of 18° , where α is limited to $\pm 90^\circ$. For each direction $\mathbf{d}_{i,j}$, radii r_k are generated between a range of $0.5 \cdot r_i$ and $1.5 \cdot r_i$ and a scaling increment of 1.1, based on the radius r_i .

Motivated by the assumption that the successive shape configuration is likely to be located along the direction \mathbf{d}_i of the ancestor, more shape configurations are generated in this area. This generation scheme of shape configurations is visualized in figure 3.5. The position $\mathbf{p}_{i,j,k,l}$ of a shape configuration is defined as

$$\mathbf{p}_{i,j,k,l} = \mathbf{p}_i + \overbrace{\frac{1}{2}(\mathbf{d}_i + \mathbf{d}_{i,j})}^A \cdot \overbrace{\left(\frac{1}{2} + l \cdot r_k\right)}^B, \quad (3.5)$$

where term A represents the step direction, weighted by the step size represented by term B, where index l ranges from 1 to n_{steps}

$$n_{steps} = \begin{cases} 6 & |\alpha| < 5^\circ \\ 3 & |\alpha| < 30^\circ \\ 2 & |\alpha| < 60^\circ \\ 1 & |\alpha| < 90^\circ \end{cases} \quad (3.6)$$

which represents the number of generated shape configurations dependent on the angle α between the direction vectors \mathbf{d}_i and $\mathbf{d}_{i,j}$.

Based on the set of all generated shape configurations, the one with the highest vesselness v is selected. This shape configuration $s(\mathbf{p}_{i,j,k,l}, \mathbf{d}_{i,j}, r_{i,j,k})$ is the base for a further refinement step, in which a second set of shape configurations is generated. This time the texture samples are generated based on sample pattern two. Again the shape configuration with the highest vesselness is selected as the successive shape configuration s_{i+1} of the given shape configuration s_i . The iterative tracking algorithm proceeds with the new basis shape configuration $s_i = s_{i+1}$, until two adjacent shape configurations fulfill the termination criterion, as defined later in this section.

Branching

Within each iteration of the tracking algorithm, the second best shape configuration, denoted as $s'_{s,j}$, with a direction vector $\mathbf{d}'_{s,j}$ differing more than 30° to the direction vector $\mathbf{d}_{i,j}$ of the best shape configuration is considered as a possible branch of the tracked vessel. After the termination of the tracking of a vessel, each shape configuration $s'_{s,j}$ of a potential branch is tracked for five iterations and the tracking algorithm is continued with the best evaluating vessel branch. The algorithm proceeds until all branches are terminated, using the additional restriction that branching is limited to a maximal depth of two.

Noise estimation

The vessel tracking algorithm uses a noise-adaptive criterion for the vessel termination. For this reason the level of noise present in the CTA volume is estimated by computing the mean absolute gray value difference $\bar{\delta}_g$ within a sample of 100.000 neighboring voxel pairs. The distance between a pair of voxels is chosen to be three voxel diameters.

To keep out lung tissue, voxels with gray values below -500 Hounsfield units (HU) are rejected.

Termination criterion

Other than the vesselness function v , which is used to select the shape configuration that optimally matches the underlying CTA dataset, the termination criterion determines if a vessel is still significantly distinguishable from the background or not. The termination is based on the assumption that a gray value difference δ_g of neighboring samples below the mean gray value difference $\bar{\delta}_g$ is most likely to originate from noise. Accordingly, a gray value difference greater than $\bar{\delta}_g$ indicates a meaningful boundary between object and background.

Each inner texture sample of a shape configuration is associated with its radially neighboring outer texture sample. For each pair the differences of the corresponding gray values is calculated. Now we can compute the fraction $frac_{below}$, which is the ratio of sample pairs below the mean gray value difference $\bar{\delta}_g$ with respect to the total number of pairs.

The identified optimal shape configuration is only accepted, if $frac_{below}$ of the shape configuration and its two ancestors is below a maximal fraction $P_{f_{below}}$ of 0.65. Otherwise the investigated optimal candidate is rejected and the tracking of the current vessel terminates. It is also terminated if the optimal candidate intersects with one of its ancestors (loop), or if the mean gray value of exterior samples drops below -500 HU. This prevents the tracking of vessels outside of the myocardial region, where the normal background gray value is significantly lower than within the myocardium.

Interpolation of centerline

After the tracking procedure has finished, the vessel centerline is only defined at discrete positions. To obtain a continuous centerline, Zambal et al. are successively fitting cubic Bézier curves between two adjacent segment positions to interpolate the vessel centerline. Figure 3.6 shows an example. Center positions \mathbf{P}_0 and \mathbf{P}_1 and normalized tangent vectors \mathbf{t}_0 and \mathbf{t}_1 are known, but for the definition of a cubic Bézier curve two additional control points \mathbf{P}_2 and \mathbf{P}_3 are needed. The calculation

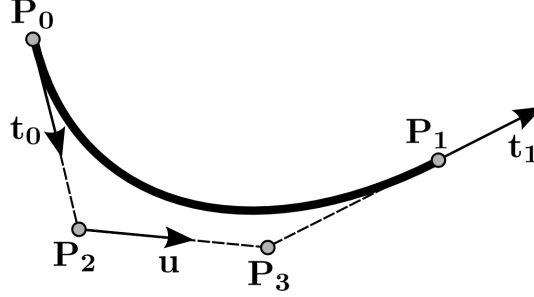


Figure 3.6: Interpolation of the centerline between two adjacent segment positions by a Bézier curve. Points \mathbf{P}_0 and \mathbf{P}_1 and corresponding normalized tangent vectors \mathbf{t}_0 and \mathbf{t}_1 are known. Two additional control points \mathbf{P}_2 and \mathbf{P}_3 can be calculated using the assumption $\|\overrightarrow{\mathbf{P}_0\mathbf{P}_2}\| = \|\overrightarrow{\mathbf{P}_2\mathbf{P}_3}\| = \|\overrightarrow{\mathbf{P}_3\mathbf{P}_1}\|$. Figure from [28].

of this control points \mathbf{P}_2 and \mathbf{P}_3 is based on the following assumption of equal distances: $\|\overrightarrow{\mathbf{P}_0\mathbf{P}_2}\| = \|\overrightarrow{\mathbf{P}_2\mathbf{P}_3}\| = \|\overrightarrow{\mathbf{P}_3\mathbf{P}_1}\|$. Let's denote the vector between \mathbf{P}_0 and \mathbf{P}_1 as vector \mathbf{v} . Then a unit vector \mathbf{u} and a scaling factor s must exist, so that

$$s \cdot \mathbf{t}_0 + s \cdot \mathbf{u} + s \cdot \mathbf{t}_1 = \mathbf{v} \quad (3.7)$$

This equation and the additional constraint that \mathbf{u} is a unit vector leads to a system of four equations. Zambal et al. remark that this system of equations is unsolvable for some possible spatial configurations, but they ensure that a solution is defined for all possible spatial configurations generated by their proposed vessel tracking algorithm.

3.2 Tree connection method of Bauer et al.

The approach of Bauer et al. [2] performs the reconstruction of complete vascular trees out of individual centerlines. The algorithm starts with the extraction of unconnected centerlines by applying a Gradient Vector Field (GVF) based tube detection. The normalization of the GVF leads to a high independence from the image contrast. Based on their assumption that blood vessels represent ridges in the Gaussian scale space, the corresponding centerlines are extracted by the use of a ridge traversal procedure.

After the extraction of the so far unconnected centerlines, the algorithm identifies potential connections between end points of centerlines and points of other centerlines by considering distance, angle and gray value difference. This way a minimum spanning forest is calculated containing the coronary artery trees. The method searches in the outward pointing tangent directions (trajectories) at end points of the centerlines for potential continuations. Based on the position of the investigated end point \mathbf{x}_S and its tangent direction \mathbf{t}_S , connection costs to other points \mathbf{x}_E of centerlines are evaluated. The connection cost function $c(\mathbf{x}_S, \mathbf{t}_S, \mathbf{x}_E)$ can be interpreted as a coned region with opening angle ρ :

$$c(\mathbf{x}_S, \mathbf{t}_S, \mathbf{x}_E) = \|\mathbf{x}_S - \mathbf{x}_E\| / \exp(-\angle(\overrightarrow{\mathbf{x}_S \mathbf{x}_E}, \mathbf{t}_S) / (2\rho^2)) \quad (3.8)$$

Points \mathbf{x}_S and \mathbf{x}_E with costs $c \leq c_{max}$ are connected, whereas potential connections with a gray value difference greater than the maximal gray value difference d_{max} are rejected. Within the MICCAI 2008 workshop this approach achieved the highest overlap measure (OV) in the category of automatic methods.

3.3 Discussion (critic) of existing approaches

Due to various reasons mentioned in section 1.3, coronary CTA data usually shows high variations in contrast along the vessels paths. Possible reasons can be present stenoses, but also image artifacts caused by motion of the beating heart during image acquisition and level of modality inherent noise with respect to small coronary artery structures. Depending on the extent of low contrast between blood vessels and the image background, the vessel tracking algorithm of Zambal et al. [28] sometimes terminates too early, although the vessel reappears with sufficient contrast in following parts. Another limitation of the algorithm is the assumption of exactly two coronary artery branches which can lead to wrong or incomplete results if anatomical variations are present.

The method of Bauer et al. uses continuous cost functions for the identification of connected vessel segments. The relation between the

angle of tangent directions, connection candidates and their distance is reflected by a single connection cost function.

The use of a single connection cost function has some disadvantages. No information about the anatomic context at the connection area is considered. For example a connection with a branch angle of more than 60 degrees may be normal for vessel tree locations near the ostium, but not for more distal parts of the vessel tree. Another important point is that expert knowledge (in this case of physicians and radiologists) is often available in the form of rules. Consider statements like "*The left coronary artery usually branches at a distance of about 5 cm from the ostium.*". This kind of expert knowledge is hard to integrate into a single cost function defined for the complete search volume. Another critical point dealing with continuous cost functions is to find a balanced coupling (weighting) of the input parameters (segment distance and angle between tangent directions).

Chapter 4

The end point: The best of two worlds

This chapter presents the new method for the detection of coronary arteries which combines the advantages of the methods of Zambal et al. [28] and Bauer et al. [2], as described and discussed in the previous chapter. This method consists of three phases, which are described in detail in the following. Figure 4.1 shows the gained results of each phase. The concrete values of the introduced constants used for the evaluation of the presented method are mentioned in section 5.

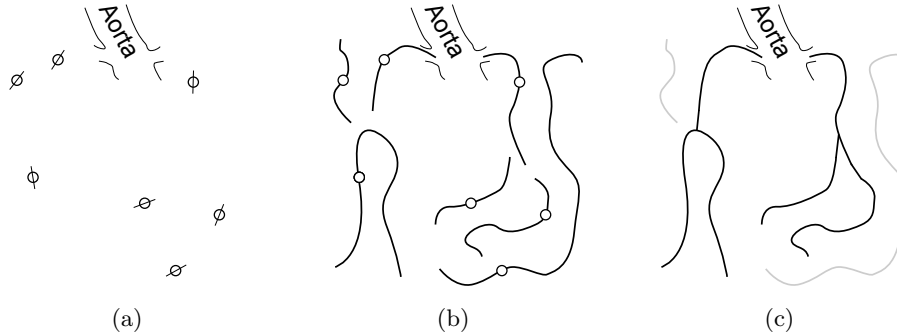


Figure 4.1: The results of the three phases of the algorithm: (a) Seed points, (b) extracted vessel segments, (c) constructed vessel tree.

4.1 Phase 1: Calculation of seed points

First we have to identify seed points in the region of the heart. These seed points are the input for the later tracking phase.

4.1.1 Calculation of the heart mask

We start with limiting the search space. This reduces not only the computation time of the seed points, but also helps to avoid tracking of vessel structures which are not belonging to the heart. Our simple approach is a combination of edge detection and first-hit raycasting. It is based on two basic assumptions:

- Assumption 1: The center of the dataset is located within the heart.
- Assumption 2: The typical threshold P_{myo} for discrimination between myocardium and lung tissue is about 500 Hounsfield units (HU).

The idea is to follow radial scan lines around the center position of the dataset. (see figure 4.2). Along each scan line we try to find the first location with a gray value below P_{myo} . If such a location can be identified, this position is likely to be part of the transition between myocardium and lung tissue.

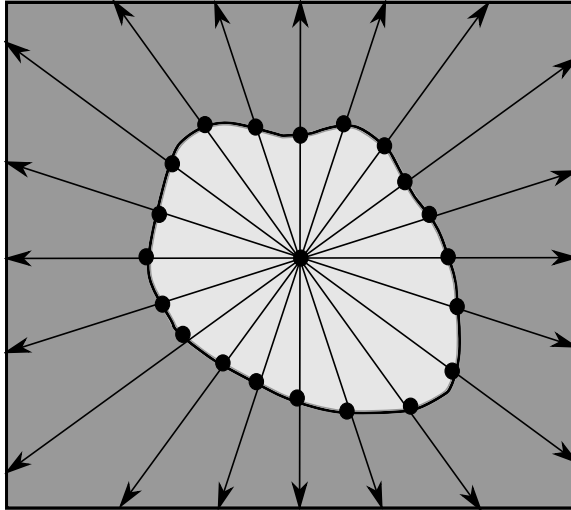


Figure 4.2: Calculation of points at the transition between myocardial and lung tissue by using radial scan lines originating from the center point of the volume.

Sometimes a significant transition between myocardium and lung tissue can not be found. This happens generally if the myocardium is

close to bone (i.e. vertebrae of the spine), so the gray value of all processed positions never drops below P_{myo} . To reduce the impact of these outliers, we interpolate the missing intersection point based on positions of successfully retrieved intersection points in the neighborhood. To prevent the accidental exclusion of coronary arteries running along the myocardium, each calculated intersection point is shifted along the outward pointing direction of the corresponding scan line by a defined constant P_{heart} . From the resulting points the heart mask is calculated by using Delaunay tetrahedrization. Please note that this ray casting approach also works in cases where the center of the dataset is located inside a heart chamber. The heart chamber is filled with blood containing contrast agent and the corresponding voxels inside the heart chamber are therefore likely to exhibit even higher gray values than the voxels of the surrounding myocardial tissue. Therefore the ray casting will not stop at the interface between heart chamber and myocardium, because both the gray values of chamber voxels and myocardium voxels are above the threshold P_{myo} .

4.1.2 Calculation of seed points

Before we can start the tracking of a vessel, we need an initial point (seed point) located inside the vessel. For this purpose we use the fact that vessels are structures of high local symmetry.

The following approach for the calculation of seed points is based on the method of Zambal et al. [28] for the detection of candidates for the coronary artery tree roots (see section 3.1.1). The method has been modified and improved in terms of generality, robustness and number of false positive results. This is due to the fact that the seed point search is extended to the complete heart region and not only the areas around the roots of the coronary artery trees. Similar to Zambal's approach we try to find vessel seed points, but we additionally extract information about the orientation and radius of the corresponding vessel segments.

The detection of vessel profiles is based on the following assumptions:

- Cross sections of vessel structures have the shape of (perfect) circles.

- Points within the vessel lumen show higher gray values than points outside of the vessel.
- Points on the circle represent the transition between vessel lumen and the background tissue and therefore exhibit a significant gradient.
- The gradient at a surface point corresponds to the surface normal and points towards the inside of the vessel.
- The identified surface point and the corresponding surface normal define a line, that approximately crosses the vessel profile through the center of the vessel lumen and intersects the vessel surface in a second point, but opposite to the identified surface point.
- The line segment between this two points represents the diameter of the vessel profile.

Based on the above assumptions, the algorithm consists of the following two steps:

1. Detect vessel profiles by circle matching, using a ray casting approach.
2. Verify the found vessel profiles by inspecting the corresponding texture values.

For every voxel at position \mathbf{p} of the volume we calculate the corresponding gradient. According to the above assumptions, the gradient corresponds to the surface normal pointing towards the center of the vessel. If the gradient of position \mathbf{p} is above a fixed threshold $P_{gradient}$, we assume that \mathbf{p} resides on a significant transition between foreground (vessel lumen) and background.

If the gradient of \mathbf{p} is below $P_{gradient}$, we skip \mathbf{p} and proceed with position \mathbf{p} of the next voxel in the dataset. Otherwise \mathbf{p} is regarded as the surface point of a vessel in the dataset and the next calculation step is to identify the intersection point \mathbf{p}' between the opposite side of the vessel profile and the line g defined by position \mathbf{p} and the corresponding gradient vector.

Point \mathbf{p}' is calculated by using a simple ray casting method (see figure 4.3(a)). First we calculate the average gray value t_{gray} at the

positions of both neighboring voxels of \mathbf{p} along the line g . Starting at \mathbf{p} , we trace the line g up to a maximum length defined by the maximum vessel diameter of 10 mm in the direction of the corresponding gradient. The searched intersection point \mathbf{p}' is now defined as the first voxel position along the scan line that exhibits a gray value below t_{gray} . If no such position is found, the algorithm skips processing of the current position \mathbf{p} and proceeds with the investigation of the next voxel in the dataset. Please note that this technique not only identifies true positive interfaces between the vessel lumen and the background, but also identifies interfaces between calcifications and the vessel lumen, which results in wrong vessel profiles. For reducing the the number of outliers, we only accept intersection points \mathbf{p}' with a minimal distance of 1.5 mm, which corresponds to the clinical relevant minimal diameter of the coronary arteries, as described in section 1.1.1. This way, vessel profiles matched at spots of calcifications are suppressed to a certain extend.

Once \mathbf{p}' is identified, the radius of the estimated vessel profile is defined as

$$r_c = \frac{1}{2} |\overrightarrow{\mathbf{p}\mathbf{p}'}| \quad (4.1)$$

and the center point of the estimated vessel profile \mathbf{p}_c is defined

$$\mathbf{p}_c = \frac{1}{2} (\mathbf{p} + \mathbf{p}') \quad (4.2)$$

Once we have estimated the center point \mathbf{p}_c and radius r_c of the vessel profile, we still need to estimate its orientation vector \mathbf{d}_c . Originating at center point \mathbf{p}_c , we generate a set of radial scan lines perpendicular to the vector $\overrightarrow{\mathbf{p}\mathbf{p}'}$, as visualized in figure 4.3(b).

By processing each scan line using the same ray casting approach and t_{gray} as in the previous step, we generate a set of points that intersect with the potential vessel surface. Figure 4.3(b) visualizes these points as small dots. If no intersection point is retrieved, the algorithm again skips the processing of position \mathbf{p} . Otherwise we select the intersection point with minimal distance to the center point \mathbf{p}_c and denote it as intersection point \mathbf{p}'' . If the fraction of the distance $\overrightarrow{\mathbf{p}\mathbf{p}'}$ and the estimated radius r_c differs not more than a certain fraction P_{radius} , so that

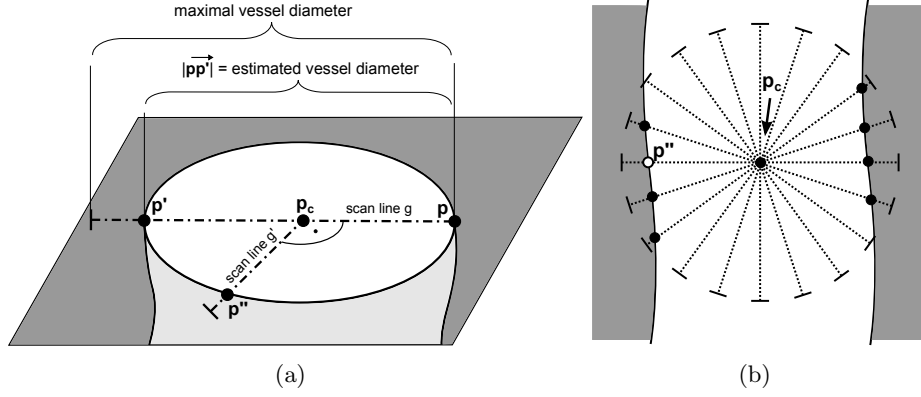


Figure 4.3: Ray casting procedure for estimation of diameter (a) and orientation (b) at the investigated voxel at position \mathbf{p} .

$$\max \left(\frac{|\overrightarrow{\mathbf{p}\mathbf{p}'}|}{r_c}, \frac{r_c}{|\overrightarrow{\mathbf{p}\mathbf{p}''}|} \right) \leq P_{radius}, \quad (4.3)$$

we calculate the circle orientation \mathbf{d}_c as the cross product between $\overrightarrow{\mathbf{p}\mathbf{p}'}$ and $\overrightarrow{\mathbf{p}\mathbf{p}''}$. The estimated vessel profile that passes through the investigated voxel at position \mathbf{p} is finally determined by center point \mathbf{p}_c , orientation vector \mathbf{d}_c and radius r_c . Next we need to evaluate if the estimated vessel profile fits to the texture values of the underlying dataset.

The evaluation of the vessel profile is based on the basic idea that voxels outside the vessel profile should also have a lower gray value than threshold t_{gray} . Therefore we sample gray values on a circle with the same center point \mathbf{p}_c and orientation \mathbf{d}_c like the estimated vessel profile, but slightly bigger with a radius r_c multiplied with factor $P_{factorOut}$. If at least a fraction of $P_{fractionOut}$ of the sampled gray values are below threshold t_{gray} , we add the calculated vessel profile to the set of initial vessel seeds for the vessel tracking procedure. Algorithm 1 shows the pseudo code for the estimation of vessel profiles for a given volumetric dataset.

4.2 Phase 2: Vessel segment tracking

The vessel tracking of the presented approach is based on the method of Zambal et al. [28], as described in section 3.1. Zambal's method

Algorithm 1 Pseudo code of the estimation of vessel profiles for a given volumetric dataset.

Input: volumetric dataset

Output: Set S_{seeds} of estimated vessel profiles

```

1: for each position  $\mathbf{p}$  in volumetric dataset do
2:   if  $\text{gradient}(p) \geq P_{\text{gradient}}$  then
3:     Define scan line  $g(x)$  at  $\mathbf{p}$  along  $\text{gradient}(\mathbf{p}_c)$ 
4:     Calculate mean gray value  $t_{\text{gray}}$  of  $\mathbf{p}$ 's neighbors along  $g(x)$ 
5:     if  $\exists \mathbf{p}'$  along  $g(x)$  with gray value  $< t_{\text{gray}}$  then
6:        $\mathbf{p}_c = \frac{1}{2} \cdot \overrightarrow{\mathbf{p}\mathbf{p}'}$ 
7:        $r_c = \frac{1}{2} \cdot |\overrightarrow{\mathbf{p}\mathbf{p}'}|$ 
8:       Generate set  $T$  of points along radial scan lines  $g'(x)$  at  $\mathbf{p}_c$  perpendicular to  $\overrightarrow{\mathbf{p}\mathbf{p}'}$ , with gray value  $< t_{\text{gray}}$ 
9:       if  $T \neq \{\}$  then
10:         $\mathbf{p}'' = \mathbf{t} \in T$  with minimal distance to  $\mathbf{p}_c$ 
11:         $\mathbf{d}_c = \overrightarrow{\mathbf{p}\mathbf{p}'} \times \overrightarrow{\mathbf{p}\mathbf{p}''}$ 
12:        if  $\overrightarrow{\mathbf{p}\mathbf{p}''} \approx r_c$  and the fraction of gray values along sampled circle defined by position  $\mathbf{p}_c$ , orientation vector  $\mathbf{d}_c$  and radius  $r = P_{\text{factorOut}} \cdot r_c$  is above fraction  $P_{\text{fractionOut}}$  then
13:           $S_{\text{seed}} = S_{\text{seed}} \cup s(\mathbf{p}_c, \mathbf{d}_c, r_c)$ 
14:        end if
15:      end if
16:    end if
17:  end if
18: end for

```

tracks the complete left and right coronary artery trees beginning from the estimated ostia down to the distal branches. In contrast to this top-down approach, the new method first tracks a set of vessels without bifurcations. The tracking of each vessel is started at promising locations in the whole heart region, represented by the set of vessel profiles calculated in the previous phase of the algorithm. This new tracking algorithm (see Algorithm 2) and the essential adaptations of the method of Zambal et al. are described in the following.

Each of the estimated vessel profiles defined by position \mathbf{p}_c , orientation vector \mathbf{d}_c and radius r_c represents a potential initial shape configuration, in the following referred to as seed configuration $s_{seed}(\mathbf{p}_c, \mathbf{d}_c, r_c)$. In order to start the tracking of vessels at the most promising seed configurations, the seed configurations are processed in descending order of their vesselness function $v(\mathbf{p}_c, \mathbf{d}_c, r_c)$ applied on the underlying CTA dataset, by usage of sample pattern one as described in section 3.1.2. Each seed configuration serves now as the initial shape configuration for the vessel tracking algorithm of Zambal et al. In contrast to Zambal's method, we track the vessel in both directions $+\mathbf{d}_c$ (forward) and $-\mathbf{d}_c$ (backward) of the seed configuration s_{seed} , which results in two subsequences of successive shape configurations, which are extended alternately within an iteration of the tracking algorithm.

The tracking for each of the two directions stops when the termination criterion is fulfilled (see below). By inverting the backward sequence and attaching the forward sequence, we obtain the final sequence of shape configurations that matches a part of a vessel in the given CTA dataset. This sequence of nodes is in the following denoted as vessel segment. The algorithm only starts tracking of seed configurations, that are not located within already tracked vessel segments.

The termination criterion follows the method of Zambal et al. as described in section 3.1.2, but the following adaptations have been made. The tracking stops at the current shape configuration, if it is located inside an already tracked vessel segment. Furthermore Zambal's method considers the sample pairs of the current shape configuration and its two ancestors. During development we observed that in regions of low contrast (mostly at distal parts of the CAs) this averaging allows the tracking of coronary artery vessel segments into venous vessel segments and vice versa. Therefore we adapted the termination criterion

Algorithm 2 Pseudo code of the vessel tracking algorithm.

Input: volumetric dataset

Input: Set S_{seeds} of estimated vessel profiles

Output: Set V of tracked vessel segments

```

1:  $V = \{\}$ 
2: Order all elements of  $S_{seeds}$  in descending order of their vesselness function  $v$  evaluated on volumetric dataset.
3: for each seed configuration  $s_{seed}(\mathbf{p}_c, \mathbf{d}_c, r_c) \in S_{seeds}$  do
4:   if  $s_{seed}$  is not located inside already tracked vessel segment in  $V$  then
5:     Initialize shape configurations  $s_f(\mathbf{p}_c, \mathbf{d}_c, r_c)$  and  $s_b(\mathbf{p}_c, -\mathbf{d}_c, r_c)$  and empty lists  $F$  and  $B$ , respectively for for- and backward tracking.
6:     while  $s_f$  or  $s_b$  not terminated do
7:       if  $s_f$  not terminated then
8:         Generate next best shape configuration  $s_{f+1}$  based on  $s_f$  as described in chapter 3.1.2.
9:         if  $s_{f+1}$  is not located inside already tracked vessel segment of  $V$  and is not fulfilling the termination criterion then
10:            $F.add(s_{f+1})$ 
11:            $s_f = s_{f+1}$ 
12:         else
13:            $terminate(s_f)$ 
14:         end if
15:       end if
16:       if  $s_b$  not terminated then
17:         Generate next best shape configuration  $s_{b+1}$  based on  $s_b$  as described in chapter 3.1.2.
18:         if  $s_{b+1}$  is not located inside already tracked vessel segment of  $V$  and is not fulfilling the termination criterion then
19:            $B.add(s_{b+1})$ 
20:            $s_b = s_{b+1}$ 
21:         else
22:            $terminate(s_b)$ 
23:         end if
24:       end if
25:     end while
26:     Vessel segment  $V_c = concat(reverse(B), s_{seed}, F)$ 
27:      $V = V \cup V_c$ 
28:   end if
29: end for

```

to consider only the current shape configuration without considering the ancestors. Furthermore the maximally allowed fraction of sample pairs below the mean gray value difference P_{below} has been reduced to 0.60 instead of 0.65. In contrast to the approach of Zambal et al. (see section 3.1.2), the new approach uses a linear interpolation of the centerline between neighboring shape models. The results of Zambal et al. show that direction vectors of successive shape models sometimes show a certain degree of freedom, which means that they do not perfectly enough align with the tangential direction of the real vessel. In these cases the cubic interpolation of the centerline between successive shape models leads to wavelike displacements of the interpolated centerline and therefore decreases the accuracy of the centerline. Therefore the centerline between the positions of two adjacent shape models is interpolated by straight line segments.

4.3 Phase 3: Topological tree growing

The result of the tracking phase is a set of unconnected and unbranched vessel segments. The goal of this final phase is to identify segments close to the ostia of the investigated vessel trees and then iteratively extend these initial trees with additional segments, until the coronary artery trees are reconstructed.

Each vessel segment represents an undirected graph without loops, where each node corresponds to a shape configuration of the iterative tracking algorithm described in the previous section. Now we can define a node path as the shortest path between a node and another node within same vessel segment of a given size, where each node has exactly the same number of node paths as its number of adjacent nodes.

4.3.1 Connection rules

Instead of a single cost function proposed by Bauer et al., we use a rule-based approach. Each of these rules represents knowledge about a certain kind of connection. The rules consider not only the relative orientation of investigated vessel segments to each other, but also additional context information like the path distance to the user-defined root node at the investigated node of the vessel tree.

We define a set of so called connection rules. A rule determines, whether one or more nodes of unconnected vessel segments (target nodes) are potential continuations of the investigated node of the vessel tree (source node). A connection rule is defined by its type and by the following set of parameters:

Search radius r_{search} : The radius around the source node within which possible target node candidates are collected.

Node path size $path_{tangent}$: The number of elements of the considered node path used for the tangent estimation.

Maximal average angle of node path α_{max} : Maximal average angle between successive edges of the investigated node path.

Maximal branch angle β_{max} : The maximally allowed angle between the tangent of a node and the tangent of a connection candidate

Maximal radii ratio $ratio_{radii}$: The maximal ratio of radii of a node and its connection candidate

Maximal path distance from root d_{root} : The maximal path distance from the source node to its corresponding root node.

Source node and target node of a connection can either be end nodes or inner nodes of vessel structures. Therefore we define three different connection cases between source nodes and target nodes:

1. I-Connection: End node of current tree connected to end node of unconnected segment
2. T-Connection: End node of current tree connected to inner node of unconnected segment
3. Y-Connection: Inner node of current tree connected to end node of unconnected segment

For each of these connection types connection rules are defined: I-Connection rules, T-Connection rules and Y-Connection rules. These rules are described in detail in the following subsections. The principle of all three rule types is the same: Given a source node a connection rule decides if suitable target nodes can be connected according to the

parameters of the rule. We only search for target nodes, if the path distance between the investigated source node and its corresponding root node is below the defined rule parameter d_{root} .

The presented tree growing method allows the definition of rules with the same type but different parameters. The rule type together with its parameter configuration is in the following referred to as rule instance. The set of rule instances that are used in the presented approach are described in section 5.1 and summarized in table 5.2.

4.3.2 I-Connection rule

An I-Connection rule can only be applied on end nodes of the current vessel tree. The rule determines, if the investigated source node should be connected to a nearby end node of an unconnected vessel segment. Figure 4.4 shows a potential I-Connection.

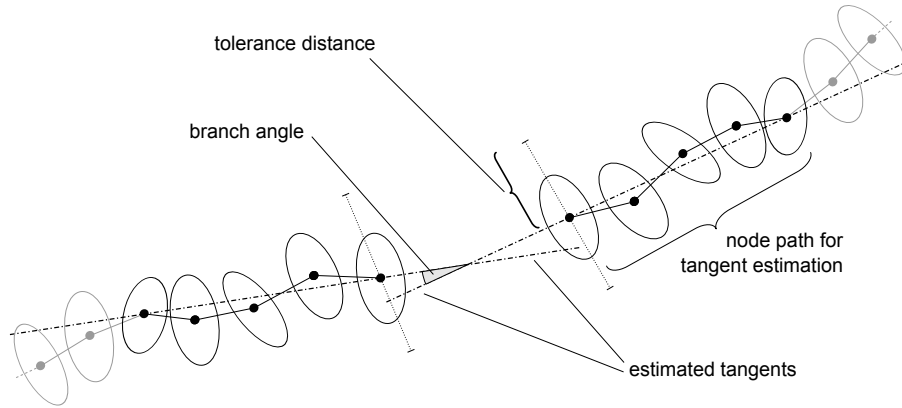


Figure 4.4: I-Connection rule: Estimation of tangential directions (dot-dashed lines) and measuring of the branching angle (gray) between the tangents at a potential connection.

The processing of the investigated source node is only proceeded, if the outward pointing tangent at the source node can be estimated by the method described in section 4.3.5. Otherwise the processing of the investigated source node is cancelled.

Next we consider end nodes of unprocessed vessel segments (target nodes) within search radius r_{search} around the position of the source node. The procedure only accepts target nodes situated at the outward pointing side of the plane, which is defined by the estimated tangent

and the position of the source node. For each found end node we estimate the outward pointing tangential direction in the same way as for the source node (see section 4.3.5). Again we ignore target nodes for which the tangent estimation delivers no result.

Now we determine if the tangent of the source node points towards the target node and vice versa. We therefore calculate the distance between the position of the investigated target node and the tangent of the source node. If the distance is greater than the vessel radius at the source node multiplied by a tolerance factor of 1.5, we reject the target node candidate. Otherwise we calculate the distance between the position of the source node and the tangent of the target node. If the distance is greater than the radius of the target node multiplied by a tolerance factor of 1.5, we also reject the investigated target node.

Among all target nodes that fulfill the above constraints, we have to identify the most appropriate node. For each target node we calculate the angle between its tangent and the tangent of the source node. The target node with the minimal tangent angle less or equal the maximal branch angle β_{max} is selected and a connection between source and target node is created. The pseudo code for the application of an I-Connection rule is shown in Algorithm 3.

4.3.3 T-Connection rule

This rule addresses connections between end nodes of the current vessel trees and inner nodes of unprocessed vessel segments. This way we handle bifurcations where the vessel segment of one branch is tracked into the other branch. An example for a possible T-Connection is shown in figure 4.5

Analog to the I-Connection rule, the tangent at the investigated source node is estimated (see section 4.3.5). Again we skip the investigation of the current source node if the estimation method returns no result.

Next we try to find the target node with the minimal tolerance distance to the tangent. Target nodes are all inner nodes of unconnected vessel segments within the defined maximal search radius r_{search} around the position of the source node. Again we accept only target nodes that are situated at the outward pointing side of the plane defined by the estimated tangential direction and position of the source node.

Algorithm 3 Pseudo code for the target node identification of the I-Connection rule.

Input: Source node n_{source} with position \mathbf{p}_s , direction \mathbf{d}_s and radius r_s

Output: Set N_{target} of identified target nodes for n_{source}

- 1: $N_{target} = \{\}$
 - 2: **if** ($rootdist(n_{source}) \leq d_{root}$) \wedge (tangent \mathbf{t}_s of n_{source} using path size $path_{tangent}$ can be estimated) **then**
 - 3: Generate sub-set of potential target nodes $N_{candidates}$ in set of nodes N_{all} of all tracked vessel segments

$$N_{candidates} = \{n_i \in N_{all} : \left. \begin{array}{ll} n_s \text{ not connected to } n_i & \wedge \\ n_i \text{ is end node of its segment} & \wedge \\ |\overrightarrow{\mathbf{p}_s \mathbf{p}_i}| \leq r_{search} & \wedge \\ \mathbf{p}_i \text{ on pos. side of plane}(\mathbf{p}_s, \mathbf{t}_s) & \wedge \\ \max\left(\frac{r_s}{r_i}, \frac{r_i}{r_s}\right) \leq ratio_{radius} & \wedge \\ distance(\mathbf{t}_s, \mathbf{p}_i) \leq 1.5 \cdot r_i & \wedge \\ \text{tangent } \mathbf{t}_i \text{ can be estimated} & \wedge \\ distance(\mathbf{t}_i, \mathbf{p}_s) \leq 1.5 \cdot r_s & \wedge \\ \angle(\mathbf{t}_s, \mathbf{t}_i) \leq \beta_{max} & \end{array} \right\} \}$$
 - 4: **if** $N_{candidates} \neq \{\}$ **then**
 - 5: $n_j = n_i \in N_{candidates}$ with minimal $\angle(\mathbf{t}_s, \mathbf{t}_i)$
 - 6: $N_{target} = \{n_j\}$
 - 7: **end if**
 - 8: **end if**
-

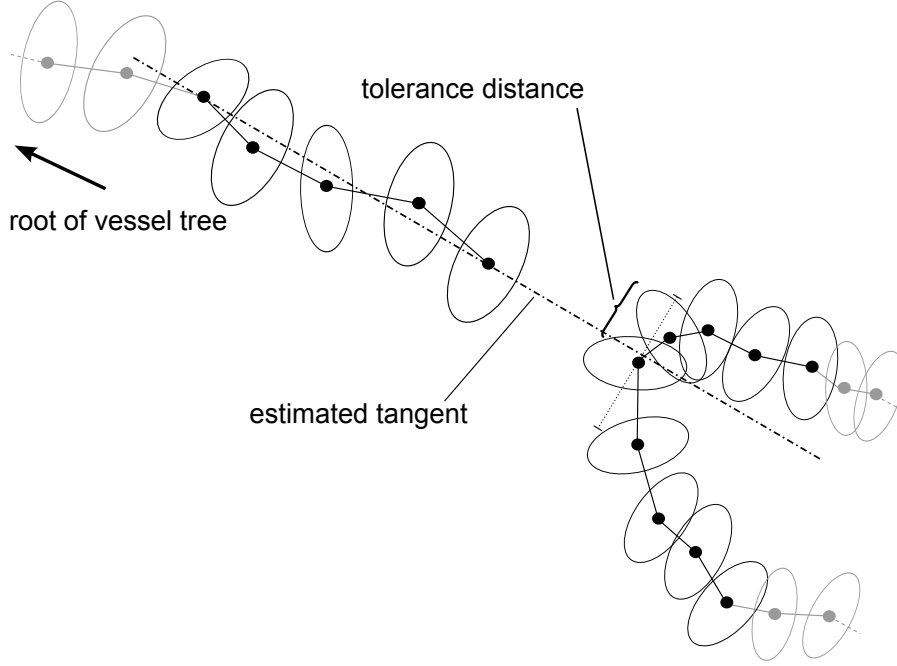


Figure 4.5: T-Connection rule: Estimation of the tangent (dot dashed line) at a possible T-Connection.

Now we check if the radii of source and target node are similar enough to be classified as nodes from the same vessel. The algorithm only accepts target nodes if the fraction of the radii of source node r_{source} and the investigated target node r_{target} differ not more than the maximal radii fraction $ratio_{radii}$

$$\max \left(\frac{r_{source}}{r_{target}}, \frac{r_{target}}{r_{source}} \right) \leq ratio_{radii} \quad (4.4)$$

defined as rule parameter. If this condition is fulfilled, we calculate the distance between the position of the investigated target node and the tangent of the source node. We proceed only if the normal distance is less than the radius of the target radius multiplied with a tolerance factor of 1.5. Among all considered target nodes, we finally choose the one with the minimal distance to the tangent of the source node.

Again we have to verify if the potential connections between the source node and the found target nodes comply with the branch angle criterion defined by the maximal branch angle β_{max} . According to the fact that we only consider inner nodes of unconnected vessel segments,

both sub-segments between the target node and the end nodes of the vessel segment have to be considered.

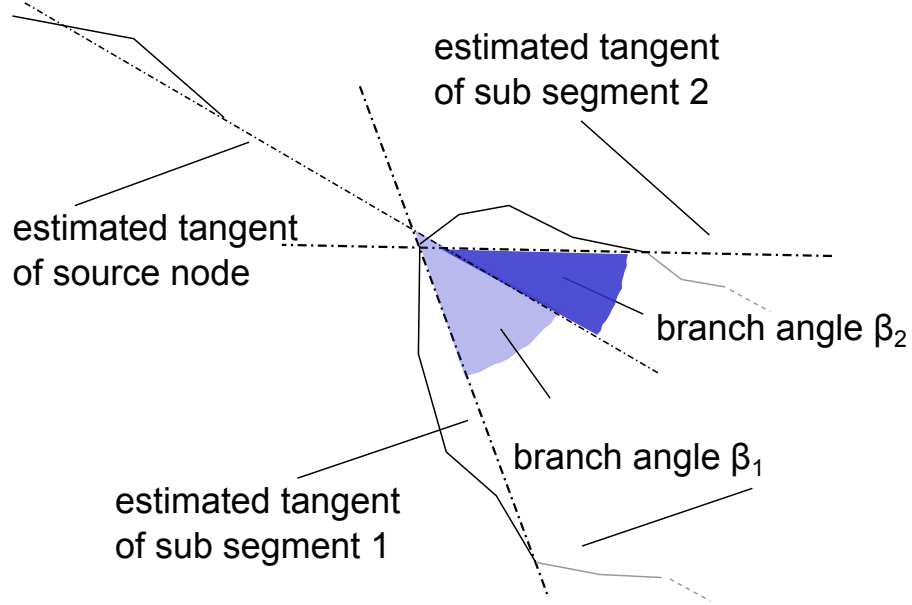


Figure 4.6: Branch angles β_1 and β_2 between tangent of source node and both sub segments of a possible T-Connection.

The estimation of the tangents of these branching segments differs from the estimation of tangents for the end nodes of segments. For each of these sub segments we consider a node path of size defined by rule parameter $path_{tangent}$, starting at the target node. We measure the angle between the tangent of the branch segment and the tangent of the source node. If both angles β_1 and β_2 of both sub segments (as shown in figure 4.6) are less or equal the maximal branch angle β_{max} the target node is finally connected to the source code. Algorithm 4 shows the pseudo code for the application of a T-Connection rule.

4.3.4 Y-Connection rule

This kind of rule is applied on inner nodes of the current vessel trees to identify connections to end nodes of unprocessed vessel segments. We search for Y-Connections by using the same logic as for T-Connections, but the other way around. This time we consider all end nodes around the source node within search radius r_{search} as possible target nodes. Again we process only target nodes for which a tangent according to the

Algorithm 4 Pseudo code for the target node identification of the T-Connection rule.

Input: Source node n_{source} with position \mathbf{p}_s , direction \mathbf{d}_s and radius r_s

Output: Set N_{target} of identified target nodes for n_{source}

- 1: $N_{target} = \{\}$
 - 2: **if** ($rootdist(n_{source}) \leq d_{root}$) \wedge (tangent \mathbf{t}_s of n_{source} using path size $path_{tangent}$ can be estimated) **then**
 - 3: Generate sub-set of potential target nodes $N_{candidates}$ in set of nodes N_{all} of all tracked vessel segments

$$N_{candidates} = \{n_i \in N_{all} : \left\{ \begin{array}{ll} n_s \text{ not connected to } n_i & \wedge \\ |\overrightarrow{\mathbf{p}_s \mathbf{p}_i}| \leq r_{search} & \wedge \\ \mathbf{p}_i \text{ on pos. side of plane}(\mathbf{p}_s, \mathbf{t}_s) & \wedge \\ \max\left(\frac{r_s}{r_i}, \frac{r_i}{r_s}\right) \leq ratio_{radius} & \wedge \\ distance(\mathbf{t}_s, \mathbf{p}_i) \leq 1.5 \cdot r_i & \end{array} \right\}\}$$
 - 4: **if** $N_{candidates} \neq \{\}$ **then**
 - 5: $n_j = n_i \in N_{candidates}$ with minimal $distance(\mathbf{t}_s, \mathbf{p}_i)$
 - 6: Calculate tangents \mathbf{t}_1 and \mathbf{t}_2 for both node paths of n_j
 - 7: **if** ($\angle(\mathbf{t}_s, \mathbf{t}_1) \leq \beta_{max}$) \wedge ($\angle(\mathbf{t}_s, \mathbf{t}_2) \leq \beta_{max}$) **then**
 - 8: $N_{target} = \{n_j\}$
 - 9: **end if**
 - 10: **end if**
 - 11: **end if**
-

method described in section 4.3.5 can be calculated. We only accept target nodes if the source node is the node with the minimal distance to the tangent of the investigated target node and the distance is less or equal the radius of the source node multiplied by a tolerance factor of 1.5. Figure 4.7 shows the application of this rule on a potential Y-Connection.

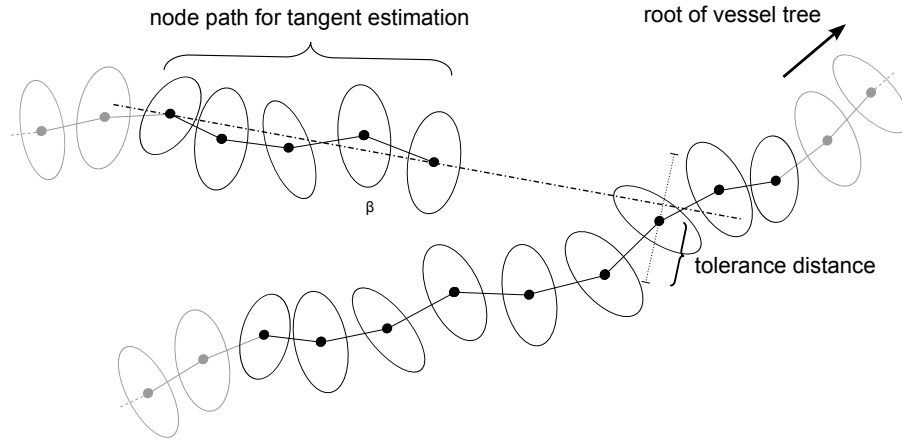


Figure 4.7: Y-Connection rule: Estimation of the tangent (dot dashed line) at a possible Y-Connection.

For each of the potential target nodes we have to evaluate if the angle between the tangents of source and target node is less or equal the maximal branch angle β_{max} . Therefore we use the same calculation of tangents like the already described T-Rule. For retrieving the tangent of the source node we consider a node path of size 4 starting at the source node. Due to the fact that the source node is part of a vessel tree, several possible paths may exist. Therefore we choose the most straightest path according to the straightness evaluation described in section 4.3.5. The tangent of the source node is represented by the vector pointing from the last node of the node path to the second node of the path. For the tangent of the target node we consider a node path of the same length starting at the target node. This time the tangent is calculated as the vector pointing from the position of the target node to the position of the last node on the node path. If the branch angle between the tangents of the source node and the potential target node are less or equal β_{max} , source and target node are connected. The pseudo code for the application of an Y-Connection rule is shown in

Algorithm 5.

Algorithm 5 Pseudo code for the target node identification of the Y-Connection rule.

Input: Source node n_{source} with position \mathbf{p}_s , direction \mathbf{d}_s and radius r_s

Output: Set N_{target} of identified target nodes for n_{source}

```

1:  $N_{target} = \{\}$ 
2: if  $rootdist(n_{source}) \leq d_{root}$  then
3:   Generate set of potential nodes
    $N_{candidates} = \{n_i \in N_{all} : \left\{ \begin{array}{l} n_i \text{ is end node of its segment} \wedge \\ |\overrightarrow{\mathbf{p}_s \mathbf{p}_i}| \leq r_{search} \end{array} \right\}\}$ 
4:   for each  $n_i \in N_{candidates}$  do
5:     Apply T-rule with  $n_i$  as input source node with same rule paramters
     as this Y-rule and retrieve the resulting set  $N_{trule}$ 
6:     if  $N_{trule} \neq \{\}$  then
7:       if  $n_{source} \in N_{trule}$  then
8:          $N_{target} = N_{target} \cup \{n_i\}$ 
9:       end if
10:    end if
11:  end for
12: end if

```

4.3.5 Tangent estimation

Starting at the end node of the investigated segment we consider a node path of size $path_{tangent}$. Because of the fact that this simple heuristic approximates the course of bended structures by lines, it should be only applied to vessel segments that show a sufficient degree of straightness. Figure 4.8 compares two node paths that show a different degree of straightness.

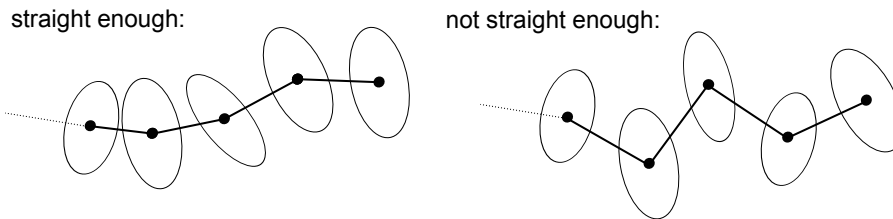


Figure 4.8: Comparison of node paths with different degrees of straightness.

Before we can search for potential continuations of end nodes of vessel segments we first need to estimate the tangent at the investigated

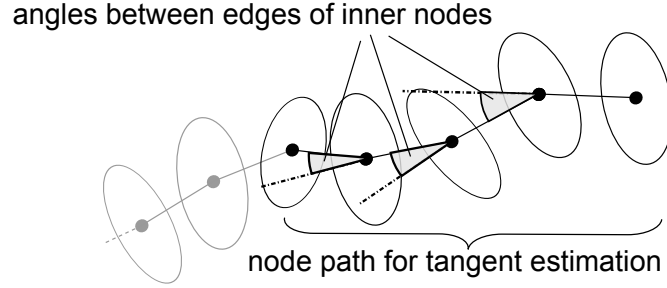


Figure 4.9: Calculation of angles between edges of inner nodes of the considered node path. Only if the mean of this angles is below α_{max} (maximal avg. angle of node path), the node path is straight enough for the estimation of the tangent.

end node. Starting from this node, we consider a node path of size $path_{tangent}$. The tangent of the end node is then defined by the position of the end node and by the vector between the position of the last node of the path and the position of the end node.

Because of this linear type of interpolation we first have to check if the investigated node path is straight enough for a reasonable direction estimation. Therefore we calculate the average angle between consecutive edges of all inner nodes of the node path, as shown in figure 4.9. The tangent is only calculated, if the average angle is less or equal the maximal average angle of node path α_{max} , defined as rule parameter. Otherwise the tangent estimation procedure and the connection rule algorithms skip the corresponding node path, as described in the rule sections above. Furthermore, if the node path traverses a node with more than two adjacent nodes, we choose the node with the minimal angle between two consecutive edges.

4.3.6 Tree growing main algorithm

In the previous section, the concept of connection rules has been presented. In the following we investigate the main algorithm of the tree growing method (see Algorithm 6).

The basic idea is the definition of a set of vessel segments that represent the initial vessel trees. Additionally we define a set of connection rules for the evaluation of possible connections. With each iteration, the algorithm extends the tree with an applicable vessel segment, until

Algorithm 6 The main routine of the tree growing algorithm.

Input: Set of root nodes, ordered set of rule instances

Output: Grown vessel tree per root node. Vessel segments at the given root nodes represent the initial vessel trees

```

1: for each  $rule_i$  do
2:   for each node of the current vessel trees  $n_{source}$  (Order by root
     distance traversal) do
3:     Retrieve set  $N_{target}$  of target nodes by applying  $rule_i$  on  $n_{source}$ 
4:     if  $N_{target} \neq \{\}$  then
5:       for each  $n_{target} \in N_{target}$  do
6:         Connect  $n_{source}$  with  $n_{target}$ 
7:       end for
8:       Restart iteration at line number 1
9:     end if
10:  end for
11: end for

```

no further unconnected vessel segment can be connected.

For the identification of the initial vessel trees, the algorithm requires the user-defined locations of the roots of the observed vessel tree structure. In the domain of coronary artery tracking, the user defines for each of the LCA and RCA tree one point right next to the ostium inside the artery. For each of these root positions, the algorithm determines the vessel segment containing the node with the minimal distance. Each identified vessel segment represents the initial coronary artery tree at the user-defined position, and the identified node represents the root node of this vessel tree. After this initialization, the algorithm extends the vessel tree in each iteration with an additional vessel segment, if one of the specified rules is applicable.

The *node traversal* of the current coronary artery trees within the application of a connection rule instance is done in a Breadth-first manner. We first visit all root nodes of the current trees. After that the next traversed node is the node with the minimal node path length between the node and its root node. Instead of traversing (and hence extending) each tree serially, we traverse all trees in a simultaneous way. This helps to avoid the connection of unprocessed vessel segments during the extension of one tree, which would actually fit better to another vessel tree.

During one iteration, we stepwise apply the defined rule instances

on the vessel tree, starting with the first defined rule in the set. The nodes of the vessel trees are visited in the described traversal-order. On each visited node, the current rule is applied. If this rule finds one (I-Connection rule & T-Connection rule) or several (Y-Connection rule) target nodes, the source node is connected with each found target node and the iteration starts from the root node with the application of the first rule on the extended vessel trees. If the application of the current rule returns no connection after processing each node of the current vessel trees, the algorithm proceeds with the next rule in the set. If no rule identifies a new connection in the current iteration, the tree growing algorithm terminates.

4.3.7 Sub-tree search algorithm

The presented main algorithm is designed to construct vessel trees starting at the vessel segments next to the user-defined roots of the observed vessel tree structures. The set of defined connection rule instances provide different heuristics for the overcoming of gaps up to a certain degree. In most of the cases this mechanism is meant to overcome local areas of low contrast for the identification and linkage of vessel segments of the observed vessel tree.

Sometimes these areas of low contrast show a much wider dimension than the defined connection rules can cover. If these wide distance gaps would be addressed with additional rules that allow gaps over long distances (by defining a high maximal search radius r_{search}), the algorithm would end up in connecting a high number of false-positive vessel structures (i.e. veins), that are not part of the artery tree.

During the development we recognized that - in some cases - coronary arteries near the ostium are not recognized by the vessel tracking algorithm in areas of very low contrast. In the more distal parts the contrast increases and the coronary artery is properly tracked by the tracking algorithm. The reconstruction of this distal part of the observed coronary artery sub-tree can be achieved with the presented vessel tree construction method. Please note that the following strategy represents a heuristic approach. Due to the fact that we search for additional tree structures of a minimal length, the approach presented in the following does not necessarily identify only coronary artery trees, but also any other elongated tree structures. Nevertheless, depending

on the clinical application of the presented tracking algorithm, these false-positive coronary artery trees may be acceptable, if at the same time true-positive sub-trees of the coronary arteries after severe occlusions and image artefacts can be identified. If such additional heuristics are used, the user should be able to easily distinguish these additionally found trees from the coronary artery trees that have been tracked based on the ostia positions, as described in the previous sections.

The basic idea of this approach is to construct vessel trees for every so far unconnected vessel segment around the user-defined root points. Then we choose the end node of the biggest calculated vessel tree as the root of an additional coronary artery sub-tree. For the identification of possible additional coronary artery sub-trees the algorithm considers end nodes within a search radius of 20 mm around the user-defined root locations of the left and right coronary artery trees. Only end nodes of vessel segments longer than 5 mm are accepted. We consider each found end node as the potential root node of a coronary artery sub tree and apply the tree growing algorithm as described in section 4.3.6. After the measurement of the total path length of the constructed vessel tree at the investigated end node, all found connections are reverted and the next end node is processed.

All end nodes with a calculated tree length below a fixed minimum tree length of 60 mm are ignored. If no end node is remaining, the sub-tree search algorithm terminates. Otherwise the end node with the maximum calculated tree length is selected. Because all of the evaluated vessel trees have been created only temporally, the vessel tree of this end node is reconstructed using the mentioned tree growing algorithm and is finally added to the so far calculated vessel trees at the user-defined root points.

Chapter 5

Implementation

The following chapter describes the assigned parameters and rule instances used in the implementation of the presented method in chapter 4, for which the algorithm produces the results that are discussed in chapter 6.

5.1 Parameters and connection rules

Our method as presented in chapter 4 has been implemented in the programming language Java. The assigned values for the introduced method parameters are summarized in table 5.1.

During analysis of the training data and the development of the algorithm we empirically defined six different connection rules for the reconstruction of the coronary artery trees. The parameters of these rules are shown in table 5.2. The main algorithm of the tree growing method (see section 4.3.6, Algorithm 6) applies the rule in the order in which they are defined. So the order of the rule instances represents the confidence of the results of different rules. For example I-Rules examine if the tangent directions of two nearby end nodes are pointing well enough towards each other. By contrast, a T-Rule considers only if the tangent directions of an end node points well enough towards an inner node of a nearby vessel segment. Therefore the I-Rule is meant to be applied first on the nodes of the current vessel trees, before the T-Rule is applied. Similarly, Y-Rules with less search radius r_{search} are applied before Y-Rules with more tolerant search radii r_{search} . In the following the different instances of connection rules are described.

Parameter	Value	Comment
P_{myo}	524 HU	Discrimination between myocardium and lung tissue
P_{heart}	2 mm	Shift calculated intersection points during heart masking along scan lines to avoid exclusion of vessel on heart surface
$P_{gradient}$	772	Minimal threshold of gray value gradient that represents a significant transition between foreground and background of a vessel profile
P_{radius}	1.2	Maximal fraction between radius r and length of vector $\vec{pp'}$ for vessel profile estimation
$P_{factorOut}$	1.1	Scaling of r_c to define outer sample circle for vessel profile evaluation
$P_{fractionOut}$	0.9	Minimum fraction of sampled gray values below threshold t_{gray} that is needed for the acceptance of an estimated vessel profile
P_{below}	0.6	Maximal fraction of gray value differences of corresponding pairs of inner and outer texture samples below mean gray value difference δ_g

Table 5.1: Summary of the chosen parameter values used in the implementation of the presented method described in chapter 4

No.	Name	r_{search}	$path_{tangent}$	α_{max}	β_{max}	$ratio_{radii}$	d_{root}
1	I-Rule	10 mm	5	12°	25°	-	-
2	I-Rule-StrongBend	2 mm	2	12°	60°	-	-
3	T-Rule	5 mm	5	22°	110°	2.0	100 mm
4	Y-Rule-SmallDist	2 mm	5	22°	120°	2.5	50 mm
5	Y-Rule-MediumDist	5 mm	5	22°	80°	2.5	-
6	Y-Rule-LargeDist	10 mm	5	22°	35°	2.5	-

Table 5.2: Table shows the order of the defined connection rules and the corresponding parameters for the vessel tree growing.

5.1.1 I-Rule

The purpose of this I-Rule instance is to find continuations of vessels across regions of low local contrast. The maximal search radius r_{search} is fixed to 10 mm and the maximal angle between the tangent directions at the investigated end nodes must not exceed the maximal branch angle $\beta_{max} = 25^\circ$.

5.1.2 I-Rule-StrongBend

Other than the previous defined I-Rule, this I-Rule instance addresses the connection of vessel segments that show strong bending. Therefore the length of the investigated node paths for the tangent direction estimation is reduced ($path_{tangent} = 2$) and the maximal branch angle has been raised ($\beta_{max} = 60^\circ$).

5.1.3 T-Rule

This connection finder instance aims for the connection of end nodes of the vessel tree with an unprocessed vessel segment representing two branches. This constellation sometimes appears at bifurcations near the root of coronary artery trees. During the vessel tracking phase a vessel segment of a branch may be tracked before the parent vessel segment at the proximal part of the bifurcation is tracked. If the tracking method evaluates cylinder candidates at the location of the bifurcation it may happen that the best evaluating cylinder models are pointing towards the other branch segment and not towards the segment connected to the vessel root. We observed that most of the T-Connections are present in areas near the vessel tree roots, hence only end nodes with a maximal root distance $d_{root} = 100$ mm are considered.

5.1.4 Y-Rule-SmallDist

The purpose of this instance is to connect branches of bifurcations near the vessel tree roots accepting wider branch angles. We only consider end nodes having a path distance from the root less or equal to $d_{root} = 50$ mm. Due to the observation that bifurcations at the very proximal regions of the artery tree (especially at the LCA) show wider branch angles than bifurcations in the distal parts we allow a more

tolerant maximal branch angle $\beta_{max} = 120^\circ$. Only connections within search radius r_{search} are permitted.

5.1.5 Y-Rule-MediumDist

This Y-Rule instance aims for the connection of branches which show a maximal branch angle $\beta_{max} = 80^\circ$ and do not exceed the maximal distance of $r_{search} = 5$ mm.

5.1.6 Y-Rule-LargeDist

This Y-Rule instance tries to identify Y-Connections in areas of low contrast. The limited maximal branch angle $\beta_{max} = 35^\circ$ allows a larger maximal distance $r_{search} = 10$ mm.

5.2 Hardware and performance

This section gives an overview of the performance. The tests have been carried out on a workstation with an Intel Core 2 Duo Processor (2.4 GHz) and 2 GB RAM. The calculation of the seed points (phase 1) takes about 10 seconds. The duration of the following tracking of the vessel segments (phase 2) varies between 8-10 minutes. The tree growing algorithm for the reconstruction of the coronary vessel trees (phase 3) takes less than 1-2 seconds.

Chapter 6

Results

This chapter presents the results obtained by the implementation proposed in the previous chapter. The chapter is organized as follows:

- Introduction of the evaluation framework (section 6.1)
- Results of the overlap and accuracy measures obtained by the presented method using the evaluation framework (section 6.2)
- Comparison of the results of the new approach with the results of the approach of Zambal et al. (section 6.3)
- Results on other medical data (section 6.4)

6.1 Evaluation Framework

Within the MICCAI 2008 conference Schaap et al. presented the "Rotterdam Coronary Artery Algorithm Evaluation Framework" [22]. The purpose of this framework is to provide an objective (and quantitative) comparison of different algorithms for the extraction of coronary arteries. The following overview of the evaluation framework closely follows the paper of Schaap et al. [22].

6.1.1 Training and test datasets

The framework involves 32 randomly selected CTA datasets. These datasets were acquired either with 64-slice or dual-source scanners and show a wide variety of image quality and degree of disease. In each dataset the centerlines of four coronary arteries were annotated by

three trained observers. Afterwards the average centerline was computed by use of a mean shift algorithm for open curves. In the next step a consensus centerline was created: Each observer compared his centerline with the averaged centerline of all observers and corrected errors if present. The corrected centerlines were used to create the reference standard of the framework.

The first 8 datasets may be used for the training, whereas the remaining 24 datasets are only used for the performance evaluation of the algorithms. All 32 datasets are published on the website of the evaluation framework, but only the reference standard centerlines of the 8 training datasets are provided. Once the tracking algorithm has been finalized, the teams can submit the calculated centerlines of the 24 test datasets via the website of the evaluation framework, where the evaluation results of the 24 test datasets are finally published.

6.1.2 Evaluation measures

The framework defines several measures for the evaluation of extracted coronary artery centerlines. The provided evaluation measures allow the discrimination between the extraction capability and the extraction accuracy of the considered extraction method.

Correspondences between centerlines

The evaluation measures are based on the point-to-point correspondences between the extracted centerline and the reference centerline. First the centerlines are equidistantly sampled using a sample distance of 0.03 mm. The extracted centerline is clipped by a disc positioned at the first point of the reference centerline, having a disc radius of twice the annotated radius and an orientation along the tangential direction at the beginning of the reference centerline. The reason for this clipping is, that the beginning of a coronary artery is defined at the ostium. Therefore no point before the first intersection of the extracted centerline with this disc is considered during the evaluation.

Definition of true positive, false positive and false negative points

The evaluation is done by classification of points on the centerlines as true positive, false positive and false negative points. This is based

on the point-to-point correspondences between the extracted centerline and the reference centerline.

A point on the reference centerline is marked as true positive TPR_{ov} if the distance to at least one of the corresponding points on the extracted centerline is below the annotated radius, and false negative FN_{ov} otherwise.

Analogous, a point on the extracted centerline is marked as true positive TPM_{ov} if the distance to at least one of the corresponding points on the reference centerline is below the annotated radius, and false positive FP_{ov} otherwise. The cardinality of a set of points is denoted with $||\cdot||$, e.g., the number of true positive points on the reference centerline is denoted as $||\text{TPR}_{\text{ov}}||$.

Overlap measures

The evaluation framework considers three different overlap measures.

Overlap OV reflects the ability to track the complete vessel.

$$\text{OV} = \frac{||\text{TPM}_{\text{ov}}|| + ||\text{TPR}_{\text{ov}}||}{||\text{TPM}_{\text{ov}}|| + ||\text{TPR}_{\text{ov}}|| + ||\text{FN}_{\text{ov}}|| + ||\text{FP}_{\text{ov}}||} \quad (6.1)$$

Overlap until first error (OF) measures how much of a vessel has been tracked until the occurrence of the first error. It is the ratio of the number of true positive points on the reference centerline before the first error (TPR_{of}) and the total number of reference points ($\text{TPR}_{\text{of}} + \text{FN}_{\text{of}}$).

$$\text{OF} = \frac{||\text{TPR}_{\text{of}}||}{||\text{TPR}_{\text{of}}|| + ||\text{FN}_{\text{of}}||} \quad (6.2)$$

Overlap with the clinically relevant part of the vessel (OT) reflects the ability of a method to track the clinical relevant part of a coronary artery. The last point of the reference centerline with a diameter larger or equal than 1.5 mm is determined. Only points on the reference centerline between this point and the beginning of the reference centerline are considered for the labelling of true positive (TPR_{ot} , TPM_{ot}), false negative (FN_{ot}) and false positive (FP_{ot}) points.

$$OT = \frac{||TPM_{of}|| + ||TPR_{of}||}{||TPM_{of}|| + ||TPR_{of}|| + ||FN_{of}|| + ||FP_{of}||} \quad (6.3)$$

Accuracy measure

Due to the reason that the evaluation should discriminate between tracking capability and tracking accuracy, the accuracy is only calculated within sections where the tracking succeeded.

Accuracy inside vessel (AI) is the average distance between corresponding points of the extracted centerline and the reference centerline, where the distance is less or equal the annotated radius of the point on the reference centerline. This measure reflects the accuracy of the centerline extraction, given that the extracted centerline lies within the vessel.

6.1.3 Scoring & ranking of the algorithms

Each of the evaluation measurements is associated with the observer performances by a relative score: 100 points if the evaluated result is perfect, 50 points if the quality of the results is similar to the performance of the observers and 0 points if the extraction completely fails. A detailed overview on the scoring method of the framework and the calculation of the observer performance is given by Schaap et al. [22].

The achieved rank of a method on a particular vessel is obtained by the comparison of the scores of all participating methods of the evaluation framework, ranging from 1 (best) to the number of participating methods (worst). The tracking capability is calculated as the average of all 288 (3 overlap measures \times 24 test datasets \times 4 vessels) related ranks. Analogously the rank of the 96 (24 test datasets \times 4 vessels) accuracy measures is obtained. The overall rank of a method is the average of the overlap and accuracy rank.

6.1.4 Algorithm categories

The evaluated algorithms are divided into three different categories according to their degree of user-interaction:

- Automatic extraction

- Extraction with minimal user interaction
- Interactive extraction

Category 1: automatic extraction

Methods within this category extract the coronary artery centerlines without any user-interaction. For the evaluation of the centerlines, two points of each reference centerline are given to select the right centerline.

- Point A: A point on the reference centerline at the distal part of the vessel. This point unambiguously defines the vessel to be tracked.
- Point B: A point on the reference centerline, situated about 3 cm distal to the beginning of the coronary artery vessel.

Point A should be used for the selection of the extracted centerline. If the result of the extraction methods does not contain a vessel near point A, point B should be used. These points are only given for the selection of the appropriate extracted centerline and must not be used during the centerline extraction algorithm.

Category 2: extraction with minimal user-interaction

In this category one point per vessel out of the following list is allowed to be used as input for the extraction algorithm.

- Point A or B: see Category 1.
- Point S: Start point of the centerline
- Point E: End point of the centerline
- Point U: any manually chosen point

In cases where the extraction algorithm produces a vessel tree from the initial point, points A and B may be used for the selection of the appropriate centerline (see category 1).

Category 3: interactive extraction

All methods that require more than one initially defined point belong to this category. They can use a series of manually chosen points, some or all points defined in category 2, or a point and a user-defined threshold.

6.2 Results

The method described in chapter 4 has been evaluated with the 24 test datasets (datasets no. 8-31) of the evaluation framework. The summary of the results are shown in table 6.1. A more detailed overview on the evaluated measures per vessel for each test datasets is shown in table 6.4 (datasets no. 8-19) and in table 6.5 (datasets no. 20-31).

Measure	% / mm			score			rank		
	min.	max.	avg.	min.	max.	avg.	min.	max.	avg.
OV	0.2%	100.0%	89.5%	0.1	100.0	53.6	1	16	8.10
OF	2.9%	100.0%	70.1%	1.7	100.0	51.7	1	16	6.90
OT	0.3%	100.0%	91.1%	0.1	100.0	64.4	1	16	6.21
AI	0.11 mm	0.78 mm	0.24 mm	7.2	76.8	47.5	1	16	2.43
Total							1	16	4.75

Table 6.1: Summary of the evaluation measures of the 24 test datasets.

6.2.1 Overlap results

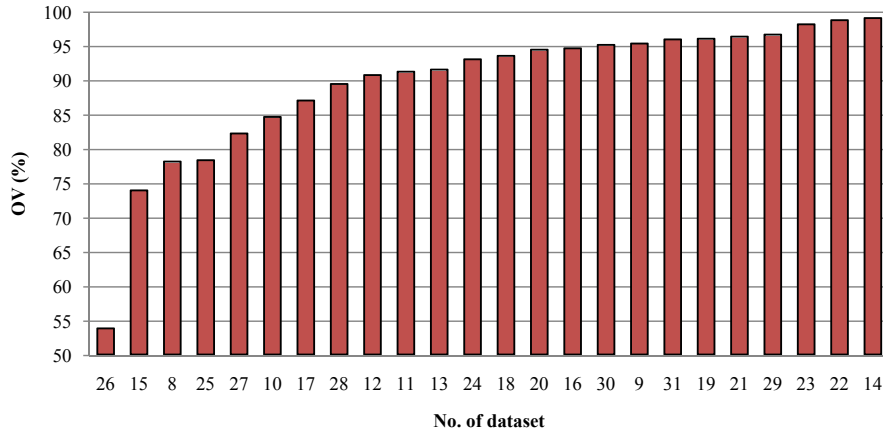
The overlap results for the 24 test datasets of the evaluation framework are shown in table 6.2. In the following we investigate the average results of the three different overlap measures.

OV

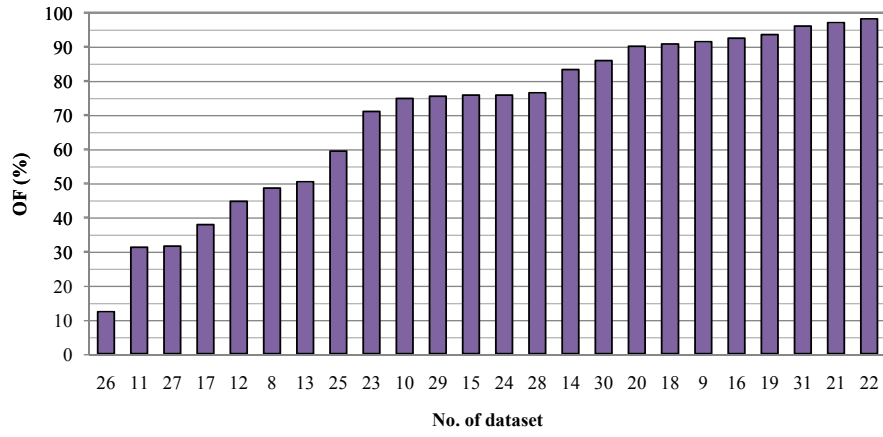
The average overlap (OV) on the test dataset is 89.5%. Figure 6.1(a) shows the OV measure per dataset, ordered by increasing OV measure. 83% of the datasets exhibit an OV measure of more than 80%.

OF

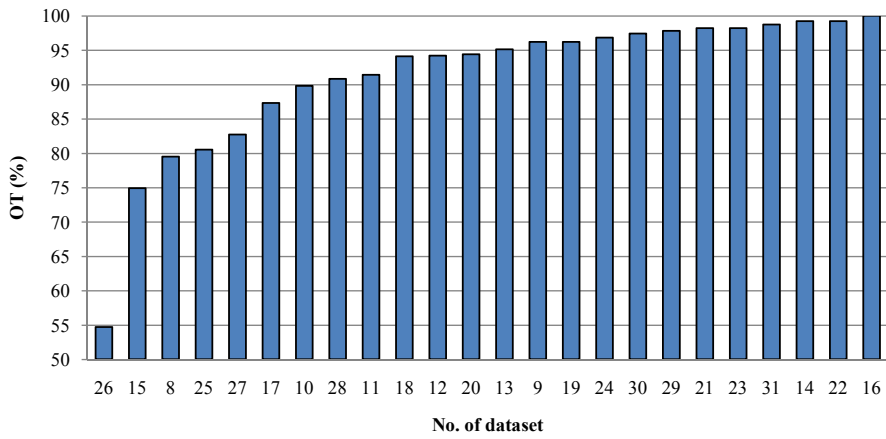
The average of the overlap until first error measure (OF) is 70.1 %. Figure 6.1(b) shows the OF measure per dataset, ordered by increasing OF measure.



(a)



(b)



(c)

Figure 6.1: Evaluated overlap measures of all 24 test datasets, ordered by increasing measures. (a) overlap (OV), (b) overlap until first error (OF), (c) overlap with clinical relevant part of the vessel (OT)

Dataset nr.	OV			OF			OT			Avg. rank
	%	score	rank	%	score	rank	%	score	rank	
8	78.1	42.1	8.75	48.5	34.5	9.25	79.5	42.3	9.25	9.08
9	95.3	60.2	7.25	91.3	63.7	6.50	96.2	73.2	6.75	6.85
10	84.6	57.6	7.75	74.7	50.9	4.50	89.8	57.9	7.50	6.60
11	91.2	46.6	8.25	31.2	30.0	6.75	91.4	46.7	8.00	7.67
12	90.7	46.8	7.25	44.6	36.3	11.25	94.2	60.2	7.00	8.50
13	91.5	46.4	10.75	50.3	26.0	10.25	95.1	47.9	10.25	10.40
14	99.0	73.4	3.75	83.2	82.0	4.25	99.2	87.2	2.25	3.40
15	73.9	44.6	11.25	75.7	62.9	8.00	74.9	62.5	8.25	9.15
16	94.6	58.0	7.75	92.4	69.7	3.75	100.0	100.0	1.00	4.17
17	87.0	44.8	9.25	37.8	19.8	10.25	87.3	44.5	9.75	9.75
18	93.5	53.3	8.50	90.7	71.3	3.75	94.1	72.6	5.00	5.77
19	96.0	74.6	6.50	93.4	85.9	4.00	96.2	86.6	3.75	4.75
20	94.4	55.6	7.50	90.0	55.8	4.50	94.4	47.6	7.50	6.47
21	96.3	50.9	8.50	96.9	79.0	5.00	98.2	63.7	6.00	6.50
22	98.7	60.2	6.50	98.0	61.6	6.50	99.2	87.1	3.00	5.35
23	98.1	54.4	7.25	70.9	60.7	7.25	98.2	74.3	4.75	6.42
24	93.0	53.5	8.25	75.7	72.2	5.25	96.8	85.9	3.00	5.50
25	78.3	39.5	9.50	59.3	42.6	4.75	80.5	52.8	7.00	7.08
26	53.8	28.2	8.50	12.3	8.6	11.00	54.7	28.7	8.50	9.35
27	82.2	43.2	9.00	31.5	18.6	11.50	82.7	42.4	8.75	9.75
28	89.4	56.4	9.75	76.4	54.0	7.50	90.8	59.2	8.75	8.68
29	96.6	71.4	5.25	75.4	50.8	5.25	97.8	86.4	2.25	4.25
30	95.1	57.5	8.50	85.8	45.0	7.75	97.4	61.9	6.50	7.58
31	95.9	68.2	9.00	95.9	58.1	6.75	98.7	74.6	4.25	6.65
Avg.	89.5	53.6	8.10	70.1	51.7	6.90	91.1	64.4	6.21	7.07

Table 6.2: Average overlap measures of the 24 test datasets.

OT

The average overlap with the clinically relevant part of the vessel (OT) is 91.1 %. Figure 6.1(c) shows the OT measure per dataset, ordered by increasing OT measure. 88% of the datasets show an OT measure of more than 80%.

6.2.2 Accuracy results

The accuracy inside vessel (AI) results for the 24 test datasets of the evaluation framework are shown in table 6.3. Figure 6.2 shows the results ordered by increasing accuracy. The average AI measure is 0.24 mm, which is significantly below the image voxel size (0.4 mm). Dataset 26 - as the only outlier - exhibits an AI measure above the image voxel size.

Dataset nr.	mm	AI score	rank	Avg. rank
8	0.24	50.7	4.00	4.00
9	0.16	50.6	1.75	1.75
10	0.26	45.4	1.50	1.50
11	0.31	45.6	3.00	3.00
12	0.24	46.1	2.50	2.50
13	0.21	50.2	1.75	1.75
14	0.28	48.8	2.50	2.50
15	0.32	41.9	5.50	5.50
16	0.20	47.4	1.50	1.50
17	0.32	47.2	4.00	4.00
18	0.19	48.9	2.50	2.50
19	0.23	50.9	2.25	2.25
20	0.34	47.2	2.00	2.00
21	0.16	46.8	2.25	2.25
22	0.19	49.4	1.25	1.25
23	0.22	46.9	2.25	2.25
24	0.14	49.2	1.50	1.50
25	0.30	43.9	2.25	2.25
26	0.49	54.9	4.00	4.00
27	0.35	41.7	3.25	3.25
28	0.15	48.6	1.25	1.25
29	0.19	46.0	1.75	1.75
30	0.18	45.9	1.50	1.50
31	0.15	45.0	2.25	2.25
Avg.	0.24	47.5	2.43	2.43

Table 6.3: Accuracy inside vessel (AI) measures of the 24 test datasets.

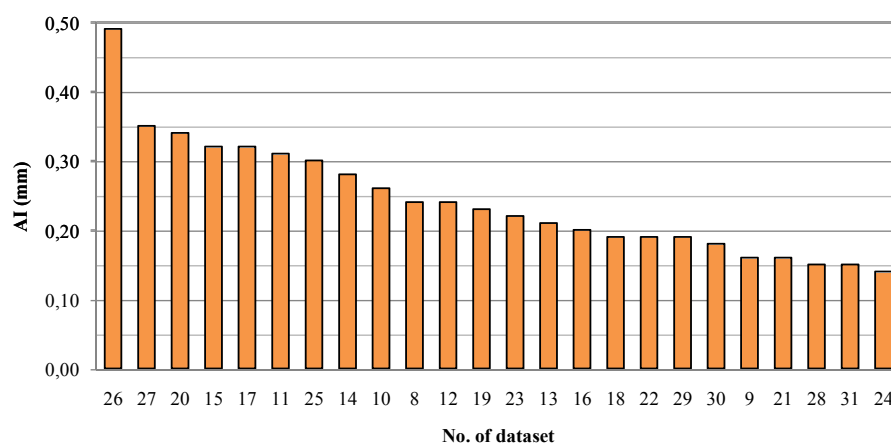


Figure 6.2: Accuracy inside vessel (AI) measures of all 24 test datasets.

6.3 Comparison to base approach

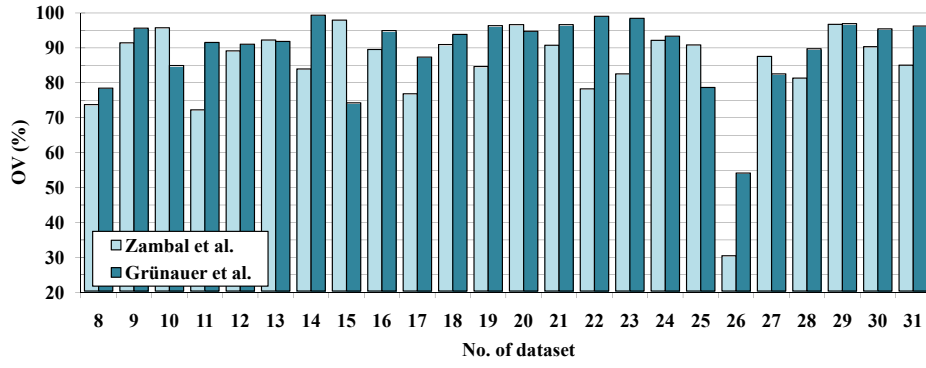
The measured average overlap OV is 89.5%, which represents an increase of 4.8% compared to the approach of Zambal et al. (with 84.7% OV). The accuracy inside vessel AI is 0.24 mm, signifying a small further improvement of 0.04 mm in comparison with the approach of Zambal et al. (0.28 mm AI). The comparison of the evaluated measures between the presented method and the approach of Zambal et al. is shown in figures 6.3(a) (OV) and 6.3(b) (AI).

Zambal et al. report a calculation time of 4 to 8 minutes per dataset, measured on a PC with Pentium 4 CPU with 3.2GHz and 2GB of RAM. As described in section 5.2, our presented method performs the tracking of the coronary artery trees in less than 10 minutes per dataset on a Intel Core 2 Duo Processor (2.4 GHz) and 2 GB RAM. The evaluation on different CPU generations inhibits a direct comparison between the computation time, but we can at least state that the computational complexity of the new approaches seems similar to the approach of Zambal et al.

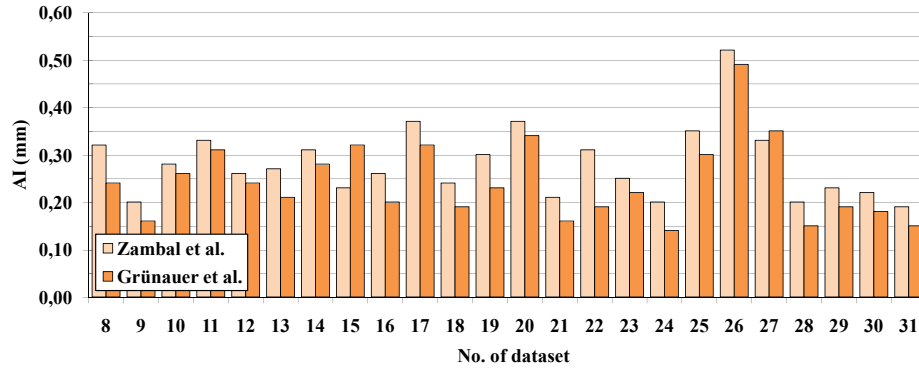
In the following sections the strong and weak points of the proposed method are presented. Section 6.3.1 addresses the most significant improvements compared to the approach of Zambal et al. The limitations of the proposed method are divided into issues of the tracking method (see section 6.3.2) and issues of the rule based connection approach (see section 6.3.3).

6.3.1 Improvements

The most prominent increase of the overlap measure OV has been achieved on dataset 26. This dataset shows a high presence of stenoses. The presented method achieved an average overlap of 53.8%, which represents almost an increase of a factor two compared to the results of the method of Zambal et al. (30.1% OV). Figure 6.4 shows the results of the three phases of the presented approach on dataset 26. Thanks to the successful application of the Y-Rule-LargeDist (see section 5.1), the RCA is tracked through a stenotic region of low contrast, which is marked by the blue arrow in figure 6.4(c). Other than the presented approach, the extraction method of Zambal et al. has not tracked these distal parts of the coronary artery. Figure 6.5 visualizes the compar-



(a)



(b)

Figure 6.3: The comparison of the evaluated measures between the presented method and the approach of Zambal et al. of the 24 test datasets: (a) overlap (OV), (b) Accuracy inside vessel (AI).

ison of the extracted centerlines between the presented approach and the method of Zambal et al.

In dataset 11 the complete branch of vessel number 3 has been tracked due to the successful application of the Y-Rule-MediumDist (see section 5.1). This branch has been missed by the approach of Zambal et al. (marked with blue arrows in figure 6.6(c) and 6.6(e)). The overlap measure OV for vessel 3 improved from 16.1% (Zambal et al.) to 93.1%. Hence the average overlap OV of dataset 11 has been increased from 71.9% (Zambal et al.) to 91.2%.

In dataset 14 the branch of vessel 3 has been tracked almost completely (OV 99.7%), whereas the method of Zambal et al. has tracked the other branch of the affected bifurcation leading to a lower overlap (OV 51.5%).

The average overlap OV of dataset 22 improved from 77.9% (Zambal et al.) to 98.7%. Similar to the previous example the improvement is based on the fact that two vessels have been tracked almost completely, whereas the tracking approach of Zambal et al. missed these two branches.

In dataset 23 the new approach enables the tracking of both branches at the bifurcation of reference vessel 2, whereas the approach of Zambal et al. tracked the branch which does not belong to the annotated reference vessel. This way the overlap OV of vessel 2 has been improved from 32.9% (Zambal et al.) to 98.7%. Hence the average overlap OV of dataset 23 increased from 82.2% (Zambal et al.) to 98.1%.

The improvements show that the novel "bottom-up" approach seems to improve tracking performance at bifurcations, where the old tracking method seems to have problems with the matching of shape models at the regions of branches. The weak matching at this areas may be due to the fact that the tracked vessel loses its tube-like appearance right at the position of a bifurcation. Assuming that phase one of the presented algorithm identifies seed points in all branches of a bifurcation, the branches will be tracked by the tracking algorithm. Further assuming that distance and orientation of the branch segments is within the constraints of one of the defined connection rules, all branches of the bifurcation will be found.

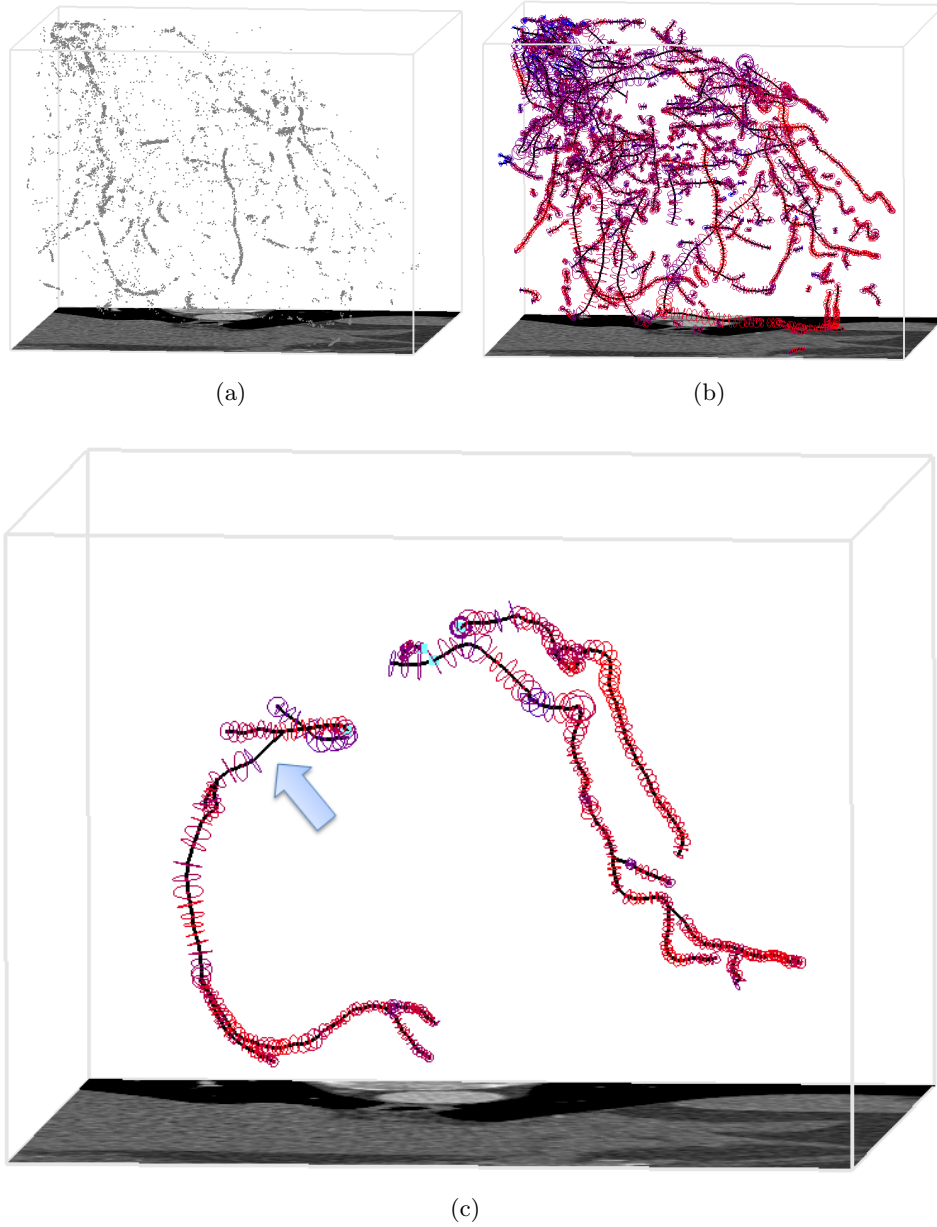


Figure 6.4: Results of the three phases of the algorithm on dataset 26: (a) calculated seed points, (b) extracted vessel segments, (c) constructed CA tree; The RCA is tracked through a stenotic region of low contrast (blue arrow) due to the successful application of the Y-Rule-LargeDist.

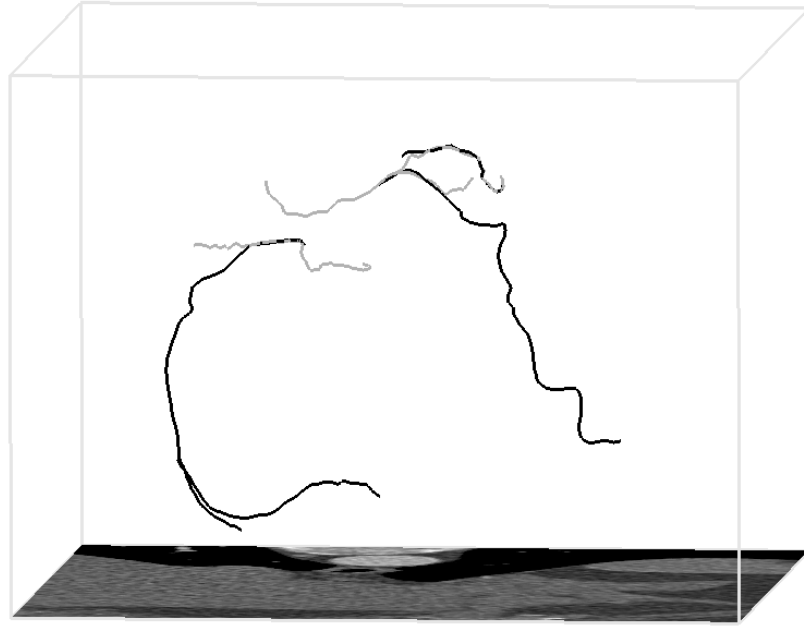


Figure 6.5: Comparison of the extracted centerlines by the method of Zambal et al. (gray) and the approach presented in this thesis (black) on dataset 26. The figure shows only the centerlines used for the evaluation.

6.3.2 Tracking issues

Some degradations of the results of the new approach are caused by the premature termination of vessel segments during the tracking phase of the algorithm. Affected locations are distal parts of the coronary arteries where the contrast between vessel and background gets lower. This premature termination has strong impacts on the decreased OV measures of datasets 20 and 25. Figures 6.6(d) (dataset 11) and 6.7(a) (dataset 20) show examples for the premature termination of two vessel segments in comparison with the extracted centerlines of Zambal et al.

Before the termination of tracking, the tracked vessel segments sometimes bend away from the real path of the vessel. Figures 6.7(b) & 6.7(c) show two examples of this kind of premature termination, occurring in dataset 27.

The observed examples of premature termination seem to be a consequence of the greedy manner of the tracking method: Once the tracking algorithm has chosen the candidate with the minimal cost value and the termination criterion is not fulfilled, the segment gets extended with

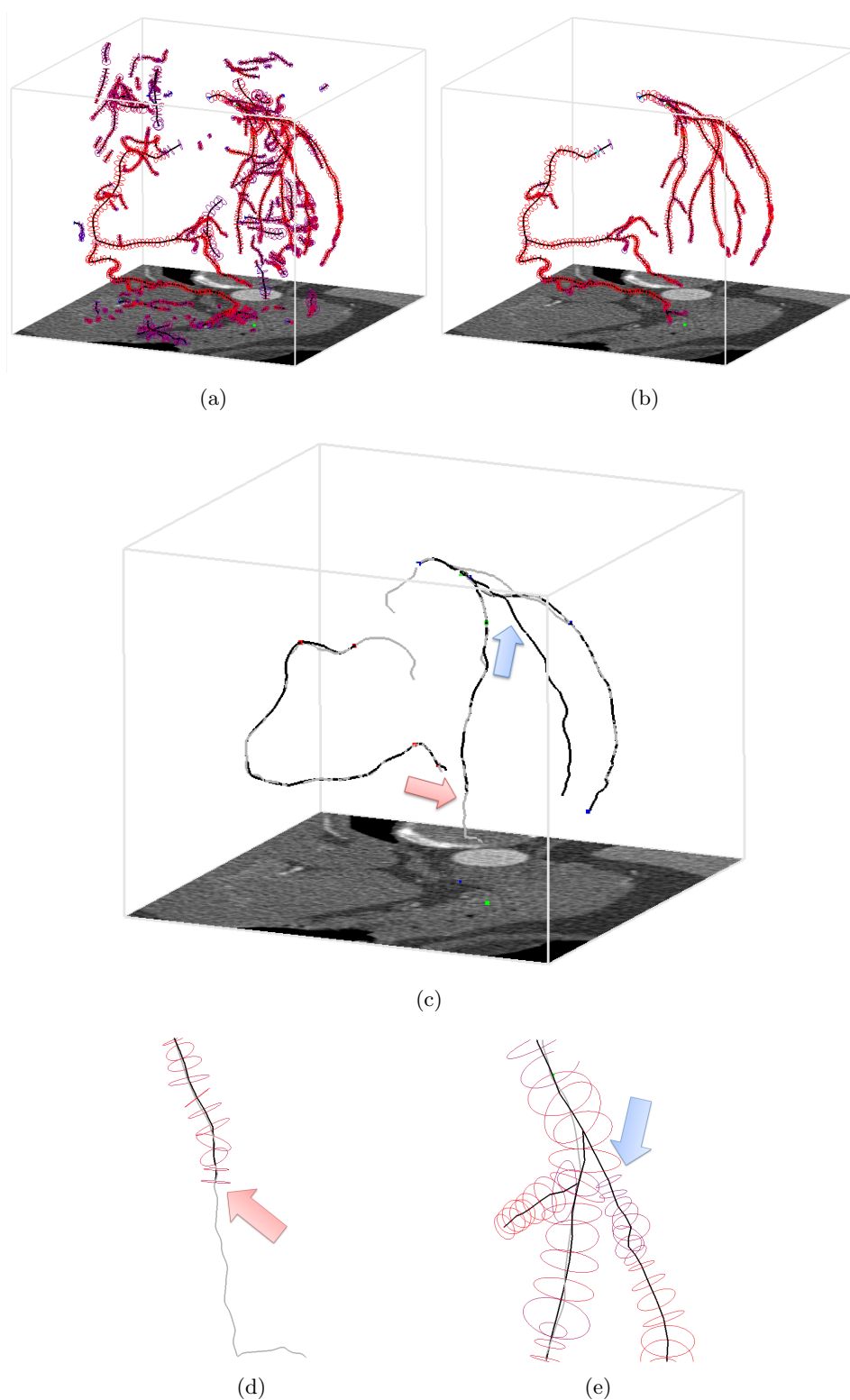


Figure 6.6: Dataset 11: (a) results of vessel tracking, (b) constructed coronary artery trees, (c) comparison of extracted centerlines between presented approach (black) and the approach of Zambal et al. (gray), (d) red arrow: premature termination of vessel segment, (e) blue arrow: successfully tracked branch that is missed by the approach of Zambal et al.

the chosen candidate. Areas of low local contrast or of high gray value (spots of calcifications) sometimes lead to a next candidate with minimal costs, but which does not properly lie on the real vessel. The outward pointing direction of the wrongly chosen candidate therefore does not point towards the continuing part of the observed vessel. In the next tracking step, none of the generated shape models will reside on the observed vessel and the tracking will stop because the measured texture will not conform to the expected values of the shape model. Due to additional bifurcation handling, the tracking algorithm of Zambal et al. indirectly overcomes cases of wrongly chosen optimal candidates by searching for possible branches at all positions of the tracked vessel segment.

A solution for both cases of premature tracking termination may be the in-depth evaluation of potential vessel paths, similar to the multiple hypothesis tracking proposed by Friman et al. [8]. The recursive evaluation of candidates up to a certain level may rise the robustness of the tracking method.

6.3.3 Rule issues

The other cases of degradations are based on the rule-based manner of the tree growing algorithm. Each rule accepts connections that meet the defined constraints like i.e. the maximal connection distance. If one of these properties of a connection exceeds the defined boundaries of the rule, the connection is not accepted.

The decreased overlap (OV) measure of Dataset 15 at vessel 2 is based on the failed application of Y-Rule-SmallDist (see section 5.1) just 2 cm after the ostium at the first bifurcation. The calculated tangent direction angle of 82.5° is greater than the defined maximal branch angle $\beta_{max} = 80^\circ$. Therefore almost the whole coronary artery is not connected to the coronary artery tree, which leads to the worst OV measure (0.2%) of all 108 vessels in the test dataset.

A similar problem occurs in dataset 25 at vessel 2. Here the T-Rule (see section 5.1) fails because one branch of the potential connection shows a branch angle of $\beta = 120^\circ$. This angle is greater than the maximal branch angle $\beta_{max} = 110^\circ$ defined by the rule and therefore the connection is rejected.

In Dataset 20 at vessel 2 the application of the defined I-Rule (see

section 5.1) fails. This connection between two end nodes of vessel segments has been rejected because both distances between each of the estimated tangent directions and the corresponding end node of the other segment are exceeding the defined tolerance distance (see section 4.3.2). The red arrow in figure 6.7(a) indicates the location of this failed connection.

This examples reveal the disadvantages of hard boundaries of the rule-based approach. Medical data in general, but especially vascular systems, show high variation, even in non-pathological cases. Some cases like the mentioned failed Y-Rule near the ostia in dataset 15 may be addressed by an additional Y-Rule with higher maximal branch angle β_{max} and a limited maximal path distance from the root d_{root} to apply this rule only at nodes near the ostium.

The analysis of the degradations show that especially the rules meant for the connection of very close vessel segments (especially bifurcations) often reject connections due the violation of the maximal branch angle. This issue may be avoided by the use of short-distance rules with more tolerant maximal branch angles.

6.4 Results on other medical data

Beside the evaluation of the presented approach within the "Rotterdam Coronary Artery Algorithm Evaluation Framework" [22] (see section 6.1), the presented algorithm has also been applied to other heart CTA datasets and the results are validated by visual inspection. Figure 6.8 shows the seed points, the tracked vessel segments and the finally obtained vessel tree. The calculated seed points as shown in figure 6.8(a) concentrate well along the coronary arteries. Especially the left coronary artery vessel tree (see figure 6.8(c)) seems to be almost completely tracked. In contrast, the tracked vessels of the right coronary artery tree seem to be terminated too soon, although the real coronary arteries in the underlying dataset seem to continue at this positions. This is possibly caused by the same tracking issues pointed out in section 6.3.2, although this can not clearly answered because no expert annotated reference centerline is available for this dataset.

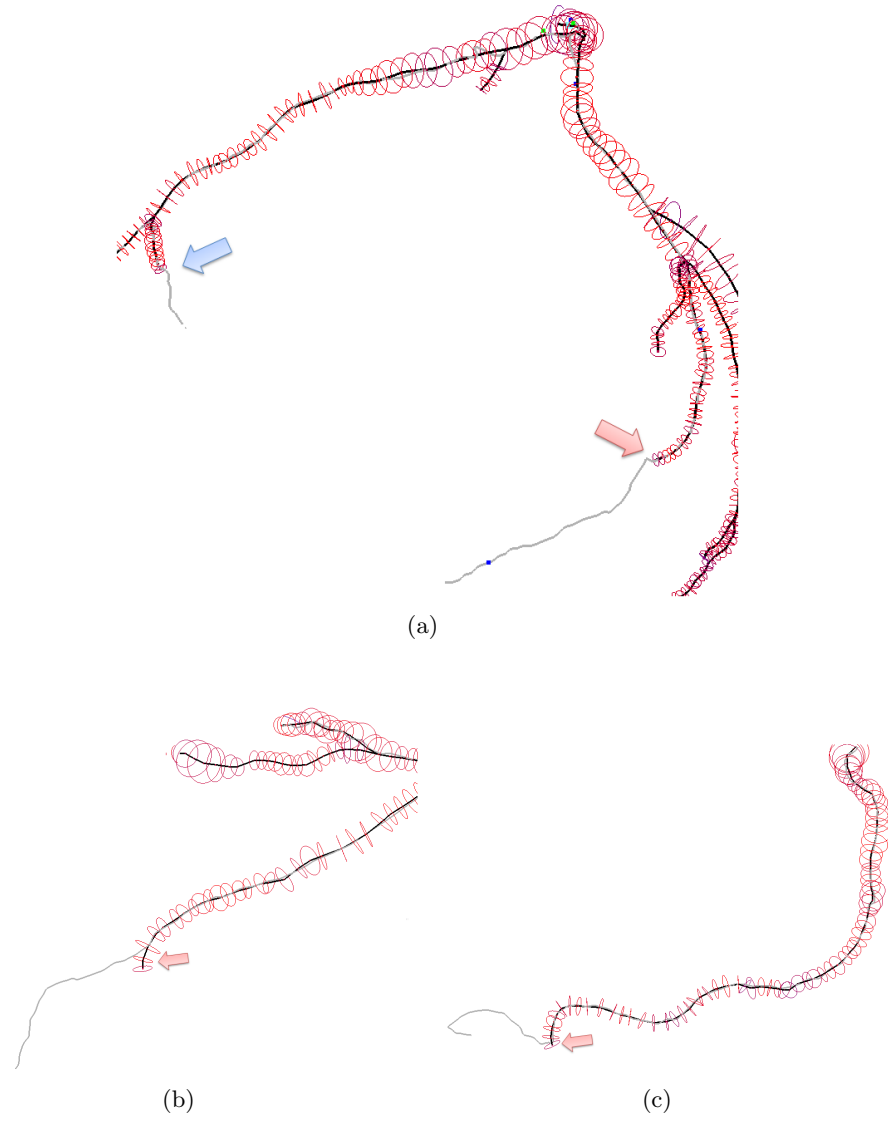
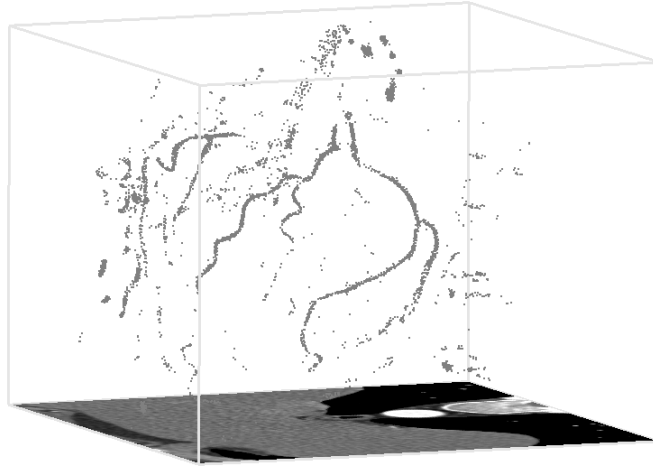
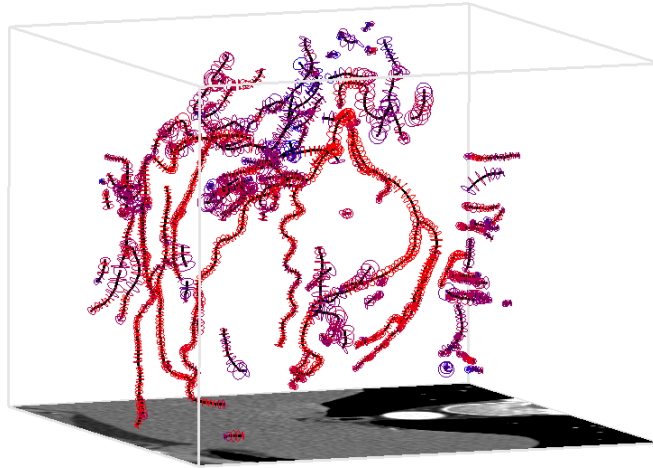


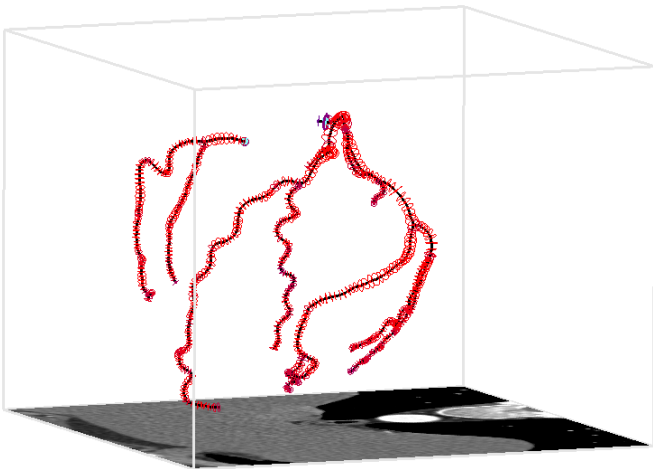
Figure 6.7: Premature termination of the vessel tracking due to the greedy manner of the tracking method: (a) dataset 20, (b-c) dataset 27.



(a)



(b)



(c)

Figure 6.8: Results on CTA dataset which is not part of the evaluation framework: (a) Seed points, (b) tracked vessel segments, (c) constructed CA trees.

D	V	OV			OF			OT			AI			Avg. rank
		%	score	rank	%	score	rank	%	score	rank	mm	score	rank	
8	0	91.8	46.5	4	80.7	41.3	8	97.5	48.8	6	0.18	48.8	1	3.5
8	1	87.3	44.5	9	3.3	1.7	16	87.3	43.7	9	0.18	45.9	4	7.7
8	2	47.4	32.3	14	35.1	49.4	9	47.4	31.8	14	0.43	51.7	10	11.2
8	3	85.7	45.1	8	75.0	45.4	4	85.7	45.0	8	0.18	56.5	1	3.8
9	0	97.0	55.5	8	94.2	48.5	6	97.0	51.6	8	0.12	52.8	1	4.2
9	1	88.0	44.5	12	78.4	41.5	11	88.0	44.1	12	0.18	49.5	2	6.8
9	2	99.0	91.1	6	98.0	84.6	5	99.7	97.2	6	0.22	44.5	2	3.8
9	3	97.2	49.8	3	94.6	80.2	4	100.0	100.0	1	0.13	55.9	2	2.3
10	0	100.0	100.0	1	100.0	100.0	1	100.0	100.0	1	0.18	45.0	2	1.5
10	1	93.4	46.7	7	41.3	20.7	6	93.4	46.7	7	0.24	43.8	1	3.8
10	2	92.1	57.0	7	85.1	46.7	4	92.3	48.3	7	0.27	50.2	2	4.0
10	3	53.1	26.6	16	72.4	36.2	7	73.4	36.7	15	0.34	42.8	1	6.8
11	0	98.8	49.4	9	6.6	3.3	12	99.7	49.9	8	0.33	39.5	5	7.3
11	1	77.5	40.8	13	12.7	50.3	4	77.5	40.8	13	0.38	46.8	4	7.0
11	2	95.4	48.5	9	86.7	45.5	10	95.4	48.3	9	0.21	48.6	1	5.2
11	3	93.1	47.9	2	19.0	20.7	1	93.1	47.9	2	0.30	47.3	2	1.8
12	0	99.6	49.9	3	100.0	100.0	1	100.0	100.0	1	0.17	42.0	3	2.3
12	1	92.8	49.0	7	6.2	4.3	16	92.8	47.6	7	0.26	45.1	3	6.5
12	2	77.8	41.7	12	63.9	36.6	12	91.6	47.2	12	0.17	54.8	1	6.5
12	3	92.7	46.6	7	8.4	4.2	16	92.3	46.1	8	0.35	42.5	3	6.7
13	0	93.9	46.9	13	19.5	9.7	14	94.8	47.4	13	0.25	47.2	3	8.2
13	1	86.3	43.5	10	92.8	47.1	7	99.8	50.0	6	0.17	50.3	2	4.8
13	2	88.0	45.6	10	78.5	42.0	8	88.0	44.9	10	0.20	52.0	1	5.2
13	3	97.9	49.7	10	10.3	5.2	12	97.9	49.5	12	0.21	51.2	1	6.2
14	0	96.8	48.9	5	33.0	28.1	14	96.8	48.9	6	0.25	52.7	3	5.7
14	1	99.3	49.7	4	100.0	100.0	1	100.0	100.0	1	0.32	43.2	2	2.0
14	2	100.0	100.0	1	100.0	100.0	1	100.0	100.0	1	0.21	55.0	3	2.0
14	3	99.7	94.9	5	100.0	100.0	1	100.0	100.0	1	0.33	44.3	2	2.2
15	0	97.2	48.7	7	100.0	100.0	1	100.0	100.0	1	0.20	54.1	3	3.0
15	1	98.8	79.6	11	100.0	100.0	1	100.0	100.0	1	0.13	54.0	2	3.2
15	2	0.2	0.1	16	3.9	2.2	16	0.3	0.1	16	0.78	7.2	16	16.0
15	3	99.4	49.8	11	98.9	49.5	14	99.4	49.7	15	0.17	52.3	1	7.2
16	0	96.9	49.0	6	94.0	48.1	4	100.0	100.0	1	0.15	53.0	2	2.8
16	1	99.2	66.5	5	98.4	92.1	6	100.0	100.0	1	0.24	45.5	2	3.0
16	2	95.1	72.6	11	100.0	100.0	1	100.0	100.0	1	0.13	48.6	1	2.7
16	3	87.0	43.8	9	77.2	38.6	4	100.0	100.0	1	0.27	42.5	1	2.8
17	0	91.1	46.9	8	40.2	22.5	11	92.4	47.5	7	0.28	51.0	3	5.8
17	1	85.2	44.7	8	19.6	10.1	5	85.2	43.3	9	0.33	46.5	2	4.7
17	2	86.3	43.9	14	76.5	39.3	12	86.3	43.9	14	0.24	47.9	2	7.7
17	3	85.2	43.6	7	14.8	7.4	13	85.2	43.4	9	0.43	43.4	9	9.3
18	0	79.7	40.3	16	81.5	41.6	12	79.7	40.3	16	0.15	52.6	2	8.3
18	1	99.7	72.7	6	100.0	100.0	1	100.0	100.0	1	0.19	46.5	5	3.8
18	2	96.7	50.7	2	81.4	43.5	1	96.7	50.0	2	0.25	44.0	2	1.8
18	3	97.7	49.8	10	100.0	100.0	1	100.0	100.0	1	0.16	52.6	1	2.5
19	0	99.7	64.6	6	100.0	100.0	1	100.0	100.0	1	0.20	53.8	2	2.3
19	1	99.5	86.2	7	100.0	100.0	1	100.0	100.0	1	0.23	52.8	1	2.0
19	2	100.0	100.0	1	100.0	100.0	1	100.0	100.0	1	0.26	47.9	4	2.5
19	3	84.8	47.4	12	73.7	43.5	13	84.8	46.2	12	0.23	49.0	2	7.2

Table 6.4: Detailed results for each of the four vessels of the evaluation measures of the test datasets 8-19.

D	V	OV			OF			OT			AI			Avg. rank
		%	score	rank	%	score	rank	%	score	rank	mm	score	rank	
20	0	99.8	80.7	4	99.8	49.9	5	99.8	49.9	4	0.21	53.0	2	3.2
20	1	98.2	49.2	5	96.4	48.2	3	98.4	49.2	5	0.36	48.5	2	3.2
20	2	84.9	42.7	15	73.9	37.3	7	84.9	42.6	15	0.26	45.6	1	6.7
20	3	94.7	49.8	6	89.9	88.0	3	94.7	48.5	6	0.51	41.7	3	4.0
21	0	95.9	49.4	10	100.0	100.0	1	100.0	100.0	1	0.12	47.4	2	3.0
21	1	93.5	47.2	12	94.1	69.2	11	96.9	48.7	11	0.16	50.1	2	6.7
21	2	99.3	57.8	5	100.0	100.0	1	99.3	57.4	5	0.15	46.8	1	2.3
21	3	96.6	49.3	7	93.4	46.7	7	96.6	48.6	7	0.23	43.0	4	5.5
22	0	99.4	49.7	8	98.9	49.4	8	100.0	100.0	1	0.16	48.4	1	3.3
22	1	96.7	49.1	8	93.7	46.9	9	96.7	48.4	9	0.20	49.7	1	4.8
22	2	99.8	92.3	5	99.6	49.9	8	100.0	100.0	1	0.23	47.3	2	3.3
22	3	98.7	49.6	5	100.0	100.0	1	100.0	100.0	1	0.18	52.2	1	1.7
23	0	99.8	49.9	4	100.0	100.0	1	100.0	100.0	1	0.21	42.4	1	1.5
23	1	99.8	49.9	8	100.0	100.0	1	100.0	100.0	1	0.22	47.2	3	3.2
23	2	98.7	69.6	7	35.5	18.1	15	98.7	49.8	7	0.24	46.3	4	6.8
23	3	94.3	48.0	10	48.1	24.8	12	94.3	47.5	10	0.21	51.8	1	5.8
24	0	98.3	66.0	8	100.0	100.0	1	100.0	100.0	1	0.12	48.5	1	2.2
24	1	84.5	43.6	11	7.0	3.5	11	87.2	43.6	9	0.16	46.0	2	6.2
24	2	98.6	57.3	5	97.2	95.3	5	100.0	100.0	1	0.17	46.5	1	2.3
24	3	90.5	47.2	9	98.5	89.9	4	100.0	100.0	1	0.13	55.7	2	3.3
25	0	96.7	48.6	6	29.7	16.5	7	99.0	49.7	8	0.24	46.2	2	4.5
25	1	26.7	13.5	15	22.6	11.3	9	26.7	13.4	15	0.52	36.5	3	8.0
25	2	98.1	49.8	8	100.0	100.0	1	100.0	100.0	1	0.18	53.0	3	3.2
25	3	91.8	46.1	9	84.9	42.6	2	96.2	48.1	4	0.27	40.0	1	3.0
26	0	78.7	42.8	8	10.2	12.2	13	82.2	45.0	8	0.41	50.2	8	8.8
26	1	25.8	13.5	10	2.9	2.1	9	25.8	13.5	10	0.43	76.8	1	5.3
26	2	31.1	15.9	11	20.6	10.7	9	31.1	15.9	11	0.61	43.6	3	6.7
26	3	79.8	40.6	5	15.6	9.6	13	79.8	40.5	5	0.50	49.1	4	5.8
27	0	89.6	44.8	9	6.2	3.1	15	91.5	45.8	8	0.35	44.6	5	7.8
27	1	60.5	34.1	12	11.9	16.4	13	60.5	34.1	12	0.41	45.1	2	7.2
27	2	93.2	49.4	5	88.0	44.2	6	93.2	46.8	5	0.25	42.5	1	3.2
27	3	85.4	44.5	10	19.7	10.7	12	85.4	42.9	10	0.40	34.5	5	7.8
28	0	91.9	46.0	14	55.1	27.5	15	91.9	46.0	15	0.12	47.8	2	8.3
28	1	87.0	45.4	9	77.1	45.4	6	89.6	46.4	9	0.13	48.2	1	4.5
28	2	79.4	44.4	10	73.6	43.2	8	81.6	44.3	10	0.19	44.2	1	5.2
28	3	99.4	90.0	6	100.0	100.0	1	100.0	100.0	1	0.15	54.2	1	1.8
29	0	95.3	47.9	8	90.9	45.7	5	100.0	100.0	1	0.13	47.8	2	3.3
29	1	91.2	45.7	6	11.2	7.8	10	91.2	45.7	6	0.21	46.2	3	5.2
29	2	100.0	100.0	1	100.0	100.0	1	100.0	100.0	1	0.21	44.3	1	1.0
29	3	99.8	92.0	6	99.7	49.9	5	100.0	100.0	1	0.20	45.7	1	2.5
30	0	94.4	47.6	9	89.7	44.9	9	100.0	100.0	1	0.13	49.3	1	3.7
30	1	95.9	78.4	7	76.9	38.7	7	95.9	48.1	7	0.17	45.9	3	5.0
30	2	94.7	48.8	11	95.6	48.5	8	96.1	49.4	11	0.21	43.8	1	5.5
30	3	95.4	55.0	7	81.0	47.8	7	97.7	50.0	7	0.21	44.7	1	4.0
31	0	89.3	44.8	15	94.2	47.1	6	100.0	100.0	1	0.11	49.4	2	4.7
31	1	96.1	48.8	5	92.5	47.4	4	96.1	48.7	6	0.15	46.0	1	3.0
31	2	99.5	96.0	7	99.0	88.6	8	100.0	100.0	1	0.15	46.5	2	3.7
31	3	98.9	83.3	9	97.8	49.3	9	98.9	49.6	9	0.19	38.0	4	6.5

Table 6.5: Detailed results for each of the four vessels of the evaluation measures of the test datasets 20-31.

Chapter 7

Integration in medical software

One part of this thesis represents the integration of the presented vessel tracking algorithm into a professional radiology workstation, which is a RIS/PACS solution of Agfa Healthcare. The general goal of such a plug-in is the extraction, visualization and analysis of the coronary artery tree for the diagnosis of coronary artery diseases by the radiologist. The plug-in prototype developed as part of this work provides the semi-automatic extraction and visualization of coronary artery trees by using the approach presented in this thesis. Furthermore it provides the functionality to track vessel segments starting at manually placed seed points. Section 7.1 gives information about the main GUI sections of the vessel tracking plug-in, whereas section 7.2 outlines the workflow of the plug-in.

7.1 Graphical user interface

The graphical user interface of the plug-in is divided into three viewing sections:

- Three views for multiplanar reconstruction
- 3D for volume rendering
- 3D view for vessel mesh rendering

In the following each of the three GUI sections (see screen shot in figure 7.1) is briefly described. Note that all views are linked. One

benefit of this feature is that, once a vessel segment gets selected in any view, all other views simultaneously highlight this vessel, if it is visible in the respective view. For example, the user can mark a vessel in one of the MPR views and immediately inspect its location in the 3D volume rendering.

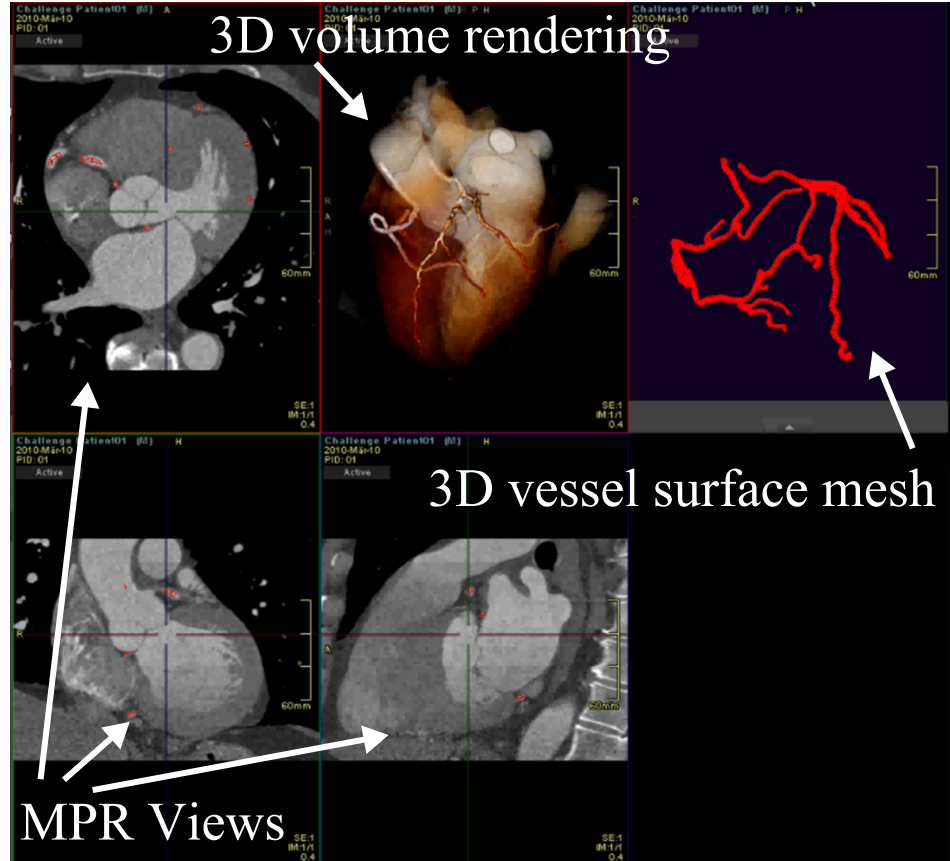


Figure 7.1: The graphical user interface of the vessel tracking plug-in integrated into a professional radiology workstation.

7.1.1 3D vessel surface mesh rendering

This view visualizes the extracted vessel tree, rendered as a 3D vessel surface mesh. The input for the calculation are the extracted center-lines of the vessel extraction algorithm described in chapter 4.

The 3D mesh is calculated in the following way. Each node of the extracted vessel segments represents a circle in the CTA dataset and is parametrized by position, direction and radius. First each circle is

approximated by a fixed number of sample points along the circle line. In a second step, the sample points of subsequent circles are connected using triangulation and are finally rendered.

The user is able to visually inspect the generated surface mesh of the extracted vessel tree, but in its current form the view is not meant for supporting medical investigation of the observed coronary artery tree. Further enrichment of the 3D vessel surface with additional information - for example colored triangles representing the calcium score of the underlying CTA dataset - may give the user a good overview on the pathological locations in the dataset.

7.1.2 MPR views

The MPR view visualizes cross section views along arbitrarily defined planes of the volume. Additionally the view outlines the cross sections of the vessel surface mesh, which is already generated as part of the previously described vessel surface mesh rendering (see section 7.1.1).

7.1.3 3D volume rendering

Beside the common visualization techniques based on transfer functions (see figure 7.2(a)), two additional visualization modes are provided. This visualization is again based on the extracted vessel centerlines. Furthermore the heart mask, obtained during the vessel tracking (see section 4.1.1), is used to remove most parts of the tissue that do not belong to the heart region.

The user can switch between these two visualization modes. The first mode highlights those voxels of the CTA dataset with blue color, which are part of extracted coronary arteries (see figure 7.2(b)).

The second mode renders voxels of the CTA dataset situated inside the 3D surface mesh opaquely, whereas the remaining voxels located inside the heart mask are rendered semi-transparently (see figure 7.2(c)). This way the user can observe the segmented vessel trees without losing information about the surrounding myocardial tissue.

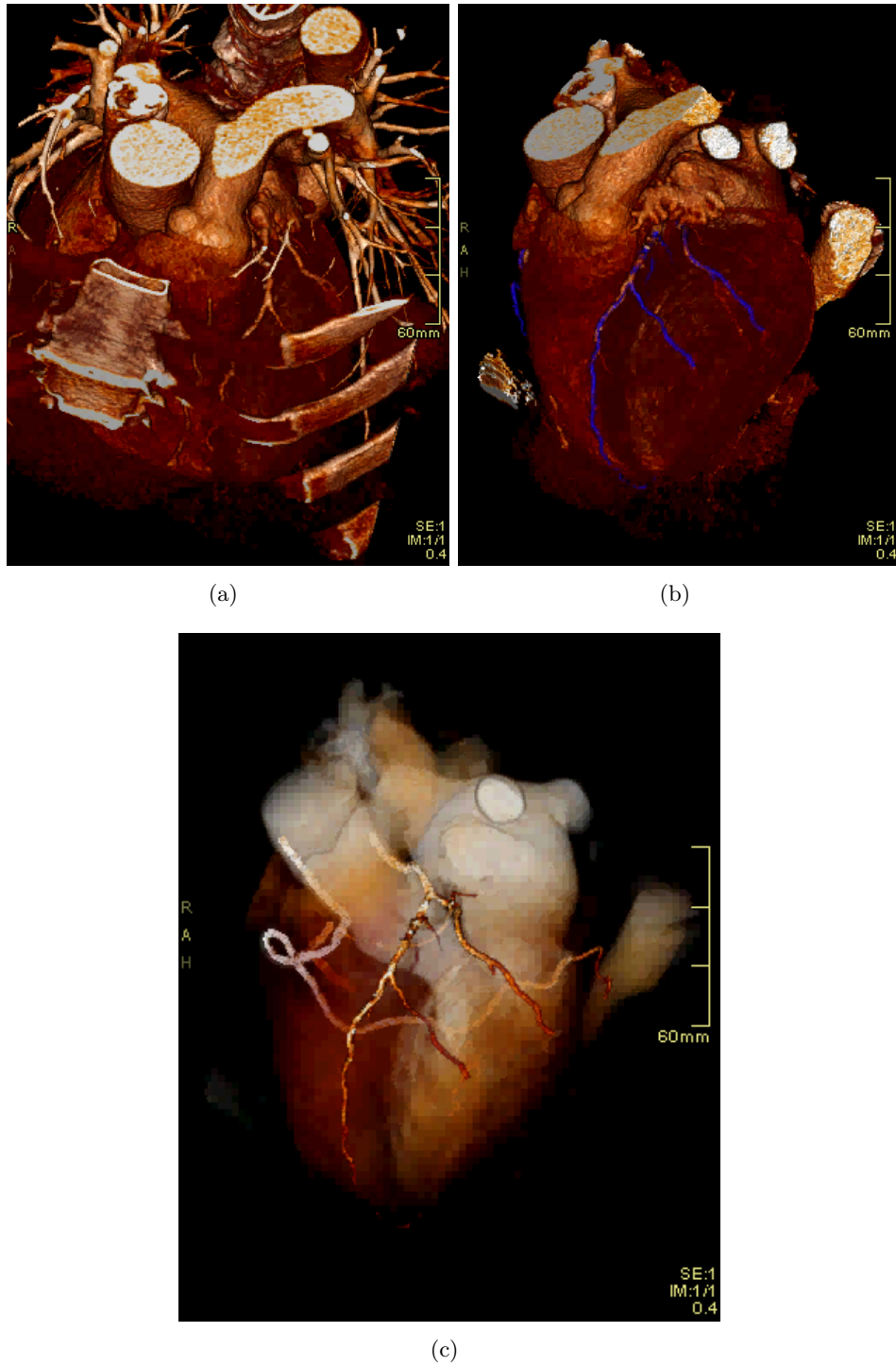


Figure 7.2: Different modes of the 3D renderer: (a) Without segmentation of heart & vessels, (b) Mode 1: rendering heart tissue and highlighted vessels (blue-colored), (c) Mode 2: rendering heart tissue transparently and vessels opaquely.

7.2 Workflow

The application of the vessel tracking plug-in on a specific patient series consists of two phases, described in the following sections.

7.2.1 (Semi-)automatic tracking

When the user activates the plug-in, the tracking algorithm gets applied on the loaded dataset. Although the presented algorithm requires minimal user interaction by defining the root points of the coronary trees in phase 3 (see section 4.3), the major parts of the calculation (phase 1 & 2) can be precalculated automatically without any interaction. If available, the precalculated vessel segments are loaded and the algorithm proceeds with phase 3. Once the user has marked the root points of the desired vessel trees, the coronary arteries originating from the given points are computed and the user can investigate the results in the provided views of the plug-in. In the case that the results of phase 1 & 2 are already available, the computation time for the calculation of the coronary artery trees takes typically less than 1-2 seconds.

7.2.2 Single-click vessel tracking

Additionally to the coronary artery trees extracted by the presented algorithm, the plug-in also provides the functionality for the tracking of vessels at manually placed seed points. This way so far undetected parts of the CA trees can be detected. The user marks a desired location for additional vessel tracking. The vessel extraction algorithm is the same as before, with the difference that now only the manually selected seed point is processed.

Chapter 8

Conclusion and Future Work

In this thesis a new approach for the extraction of coronary artery centerlines was discussed.

The main focus on this thesis lies in an approach delivering highly accurate results in combination with a high overlap of the investigated vessel tree. The novel method is divided into three phases:

- Calculation of seed points
- Vessel tracking
- Topological tree growing

Every phase operates on the output of the previous phase, so the substitution and adaptation of each phase is easily possible. A detailed description of all three phases was given in this thesis.

It was shown that the novel approach reaches a high overlap in combination with a very high accuracy. The achieved results were evaluated by a quantitative evaluation framework. Improvements but also degradations of the novel method in comparison with the base approach were discussed in detail. It has been pointed out that the balancing of the rules applied during tree growing is a critical task. Additionally the integration of the developed algorithm into clinical software was demonstrated.

Further improvements of particular phases of the presented algorithm may be covered in future work. Potential improvements are:

- *In-depth evaluation of potential vessel paths in the tracking phase:*
This may increase the robustness of the tracking method against premature termination.

- *Calibration of the connection rules in tree growing:* Further experiments in varying the number and parametrization of connection rules may help to construct the complete vessel trees.
- *Automatic root point selection:* Detection of additional anatomical structures, especially the aorta, can help to identify the root points of the coronary artery trees fully automatically.

Bibliography

- [1] S. Aylward, S. Pizer, D. Eberly, and E. Bullitt. Intensity ridge and widths for tubular object segmentation and description. In *Proceedings of the 1996 Workshop on Mathematical Methods in Biomedical Image Analysis (MMBIA '96)*, pages 131–138, Washington, DC, USA, 1996. IEEE Computer Society.
- [2] C. Bauer and H. Bischof. Edge based tube detection for coronary artery centerline extraction. In *The Midas Journal, MICCAI Workshop - Grand Challenge Coronary Artery Tracking*, 2008.
- [3] S. Bock, C. Kühnel, T. Boskamp, and H.-O. Peitgen. Robust vessel segmentation. In *Society of Photo-Optical Instrumentation Engineers (SPIE) Conference Series*, volume 6915, pages 391–399, 2008.
- [4] J. Bogaert, S. Dymarkowski, and A. M. Taylor. *Clinical Cardiac MRI: With Interactive CD-ROM (Medical Radiology: Diagnostic Imaging)*, chapter 14, pages 381–383. Springer, 2005.
- [5] B. Bouraoui, C. Ronse, J. Baruthio, N. Passat, and P. Germain. Fully automatic 3D segmentation of coronary arteries based on mathematical morphology. In *Proceedings of the 2008 IEEE International Symposium on Biomedical Imaging (ISBI'08)*, pages 1059–1062, 2008.
- [6] C. Castro, M. A. Luengo-Oroz, A. Santos, and M. J. Ledesma-Carbayo. Coronary artery tracking in 3D cardiac CT images using local morphological reconstruction operators. In *The Midas Journal, MICCAI Workshop - Grand Challenge Coronary Artery Tracking*, 2008.

- [7] S. Eiho, H. Sekiguchi, T. Sugimoto, and S. Urayama. Branch-based region growing method for blood vessel segmentation. In *Proceedings of XXth Congress of the International Society for Photogrammetry and Remote Sensing (ISPRS'04)*, pages 796–801, 2004.
- [8] O. Friman, C. Kühnel, and H.-O. Peitgen. Coronary centerline extraction using multiple hypothesis tracking and minimal paths. In *The Midas Journal, MICCAI Workshop - Grand Challenge Coronary Artery Tracking*, 2008.
- [9] K. M. Hanson. *Radiology of the Skull and Brain*, volume 5, chapter 113. Noise and contrast discrimination in computed tomography, pages 3941–3955. Mosby, 1981.
- [10] U. Hoffmann, A. J. Pena, R. C. Cury, S. Abbata, M. Ferencik, F. Moselewski, U. Siebert, T. J. Brady, and J. T. Nagurney. Cardiac CT in emergency department patients with acute chest pain. *Radiographics*, 26(4):963–978, 2006.
- [11] A. Kanitsar, D. Fleischmann, R. Wegenkittl, P. Felkel, and M. E. Gröller. CPR - Curved Planar Reformation. In *IEEE Visualization 2002*, pages 37–44, 2002.
- [12] J. Kaufhold, P. Tsai, P. Blinder, and D. Kleinfeld. Threshold relaxation is an effective means to connect gaps in 3D images of complex microvascular networks. In *Proceedings of the 3rd Workshop on Microscopic Image Analysis with Applications in Biology (MIAAB'08)*, 2008.
- [13] C. Kirbas and F. Quek. A review of vessel extraction techniques and algorithms. *ACM Computing Surveys*, 36:81–121, June 2004.
- [14] K. Krissian, H. Bogunovic, J. Pozo, M. Villa-Uriol, and A. Frangi. Minimally interactive knowledge-based coronary tracking in CTA using a minimal cost path. In *The Midas Journal, MICCAI Workshop - Grand Challenge Coronary Artery Tracking*, 2008.
- [15] D. Lesage, E. D. Angelini, I. Bloch, and G. Funka-Lea. A review of 3D vessel lumen segmentation techniques: Models, features and extraction schemes. *Medical Image Analysis*, 13(6):819 – 845, 2009.

- [16] M. A. Luengo-Oroz, M. J. Ledesma-Carbayo, J. J. Gómez-Diego, M. A. García-Fernández, M. Desco, and A. Santos. Extraction of the coronary artery tree in cardiac computer tomographic images using morphological operators. In *Proceedings of 4th International Conference on Functional Imaging and Modeling of the Heart (FIMH'07)*, pages 424–432, 2007.
- [17] D. B. Mark, D. S. Berman, M. J. Budoff, J. J. Carr, T. C. Gerber, H. S. Hecht, M. A. Hlatky, J. M. Hodgson, M. S. Lauer, J. M. Miller, R. L. Morin, D. Mukherjee, M. Poon, G. D. Rubin, and R. S. Schwartz. ACCF/ACR/AHA/NASCI/SAIP/SCAI/SCCT 2010 Expert Consensus Document on Coronary Computed Tomographic Angiography: A Report of the American College of Cardiology Foundation Task Force on Expert Consensus Documents. *Circulation (Journal of the American College of Cardiology)*, 121(22):2509–2543, 2010.
- [18] C. Metz, M. Schaap, A. van der Giessen, T. van Walsum, and W. Niessen. Edge based tube detection for coronary artery centerline extraction. In *The Midas Journal, MICCAI Workshop - Grand Challenge Coronary Artery Tracking*, 2008.
- [19] L. Risser, F. Plouraboué, and X. Descombes. Gap filling in 3D vessel like patterns with tensor fields - application to high resolution computed tomography images of vessel networks. In *Proceedings of the Second International Conference on Computer Vision Theory and Applications (VISAPP'07)*, pages 46–52, 2007.
- [20] L. Risser, F. Plouraboué, and X. Descombes. Gap filling of 3-D microvascular networks by tensor voting. *IEEE Transactions on Medical Imaging*, 27(5):674–687, 2008.
- [21] V. L. Roger, A. S. Go, D. M. Lloyd-Jones, R. J. Adams, J. D. Berry, T. M. Brown, M. R. Carnethon, S. Dai, G. de Simone, E. S. Ford, C. S. Fox, H. J. Fullerton, C. Gillespie, K. J. Greenlund, S. M. Hailpern, J. A. Heit, P. M. Ho, V. J. Howard, B. M. Kissela, S. J. Kittner, D. T. Lackland, J. H. Lichtman, L. D. Lisabeth, D. M. Makuc, G. M. Marcus, A. Marelli, D. B. Matchar, M. M. McDermott, J. B. Meigs, C. S. Moy, D. Mozaffarian, M. E.

- Mussolino, G. Nichol, N. P. Paynter, W. D. Rosamond, P. D. Sorlie, R. S. Stafford, T. N. Turan, M. B. Turner, N. D. Wong, and J. Wylie-Rosett. Heart disease and stroke statistics—2011 update: A report from the american heart association. *Circulation (Journal of the American College of Cardiology)*, 123(4):e18–209, 2011.
- [22] M. Schaap, C. T. Metz, T. van Walsum, A. G. van der Giessen, A. C. Weustink, N. R. Mollet, C. Bauer, H. Bogunovic, C. Castro, X. Deng, E. Dikici, T. O'Donnell, M. Frenay, O. Friman, M. H. Hoyos, P. H. Kitslaar, K. Krissian, C. Kühnel, M. A. Luengo-Oroz, M. Orkisz, Örjan Smedby, M. Styner, A. Szymczak, H. Tek, C. Wang, S. K. Warfield, S. Zambal, Y. Zhang, G. P. Krestin, and W. J. Niessen. Standardized evaluation methodology and reference database for evaluating coronary artery centerline extraction algorithms. *Medical Image Analysis*, 13(5):701–714, 2009.
- [23] H. Scheffel, H. Alkadhi, A. Plass, R. Vachenaue, L. Desbiolles, O. Gaemperli, T. Schepis, T. Frauenfelder, T. Schertler, L. Husmann, J. Grunenfelder, M. Genoni, P. Kaufmann, B. Marincek, and S. Leschka. Accuracy of dual-source ct coronary angiography: first experience in a high pre-test probability population without heart rate control. *European Radiology*, 16:2739–2747, 2006.
- [24] A. Szymczak, A. Stillman, A. Tannenbaum, and K. Mischaikow. Coronary vessel trees from 3d imagery: A topological approach. *Medical Image Analysis*, 10(4):548–559, 2006.
- [25] H. Tek, M. A. Gülsün, S. Laguitton, L. Grady, D. Lesage, and G. Funka-Lea. Automatic coronary tree modeling. In *The Midas Journal, MICCAI Workshop - Grand Challenge Coronary Artery Tracking*, 2008.
- [26] M. Termeer, J. O. Bescos, M. Breeuwer, A. Vilanova, F. Gerritsen, and E. Gröller. CoViCAD: Comprehensive visualization of coronary artery disease. *IEEE Transactions on Visualization and Computer Graphics*, 13:1632–1639, 2007.
- [27] G. Yang, A. Bousse, C. Toumoulin, and H. Shu. Multiscale tracking algorithm for the coronary extraction in MSCT angiography.

28th Annual International Conference of the IEEE Engineering in Medicine and Biology Society (EMBS '06), 1:3066–3069, 2006.

- [28] S. Zambal, J. Hladuvka, A. Kanitsar, and K. Bühler. Shape and appearance models for automatic coronary artery tracking. In *The Midas Journal, MICCAI Workshop - Grand Challenge Coronary Artery Tracking*, 2008.